JGR Space Physics

RESEARCH ARTICLE
10.1029/2023JA031428

Key Points:

- Inherent periodicities in Total Electron Content (TEC) time series at pairs of geo-magnetically conjugate land-locked and sea-locked stations are presented
- Thermosphere-Ionosphere-Electrodynamics General Circulation Model (TIE-GCM) accurately models semi-annual and annual oscillations, but dissimulate seasonal anomaly at southern low-latitudes
- TEC quasi biannual oscillations are coherent with solar activity variation and the 120- and 500-day periodicities appeared inside EIA crest

Supporting Information:

Supporting Information may be found in the online version of this article.

Correspondence to:

S. S. Rao,
ssraophy116@gmail.com;
sardar@prl.res.in

Citation:

Rao, S. S., Chakrabarty, D., & Srivastava, N. (2023). Solar hysteresis pattern and spectral components in TEC time series (GPS and TIE-GCM) of the quadrilaterally coupled geomagnetic conjugate low-latitude stations. *Journal of Geophysical Research: Space Physics*, *128*, e2023JA031428. https://doi.org/10.1029/2023JA031428

Received 24 FEB 2023
Accepted 15 APR 2023

Author Contributions:

Conceptualization: D. Chakrabarty, Nandita Srivastava
Formal analysis: S. S. Rao
Investigation: S. S. Rao
Methodology: S. S. Rao
Project Administration: Nandita Srivastava
Software: S. S. Rao
Supervision: Nandita Srivastava
Visualization: D. Chakrabarty
Writing – original draft: S. S. Rao
Writing – review & editing: S. S. Rao, D. Chakrabarty, Nandita Srivastava

Solar Hysteresis Pattern and Spectral Components in TEC Time Series (GPS and TIE-GCM) of the Quadrilaterally Coupled Geomagnetic Conjugate Low-Latitude Stations

S. S. Rao[1], D. Chakrabarty[2], and Nandita Srivastava[1]

[1]Udaipur Solar Observatory, Physical Research Laboratory, Udaipur, India, [2]Space and Atmospheric Sciences Division, Physical Research Laboratory, Ahmedabad, India

Abstract The current study is a first-of-its-kind in that it compares the Total Electron Content (TEC) of the solar cycle from the Global Positioning System (GPS) and Thermosphere-Ionosphere-Electrodynamics General Circulation Model (TIE-GCM) over the geomagnetically conjugate low-latitude stations with the particular scenario of lower atmospheric conditions over land- and sea-locked locations. For this, TEC data for the period 2009–2017 is used from northern hemispheric stations Varanasi (25.31°N; 82.97°E) and LHAZ (29.65°N; 91.10°E) and southern hemispheric stations DGAR (7.27°S; 72.37°E) and COCO Island (12.18°S; 96.83°E). The solar cycle variation in TEC is identified by two distinct maxima and hysteresis between the ascending and descending phases. The solar cycle trends are modulated by the equatorial ionization anomaly as well as longitudinal biases. The Lomb-Scargle periodogram shows that the improved TIE-GCM version 2.0, which incorporates variable eddy diffusion to provide an accurate simulation of seasonal variability, is largely successful in simulating semi-annual and annual oscillations but still needs to resolve the seasonal anomaly feature, particularly in the case of southern low latitude stations. Terannual (120-day) and 1.4-year (500-day) periodicities in the TEC time series are observed only at EIA region stations, not at off-crest location LHAZ, and are most likely caused by E x B drift. The wavelet coherence analysis reveals that the Quasi Biannual Oscillations (QBO) in the TEC time series (597-, 773-, and 930-day) have a strong physical affinity with the QBO oscillation of F10.7 flux. Results indicate that both solar activity and equatorial electrodynamics significantly influence the QBO oscillation in the TEC.

1. Introduction

The solar radiation reaching the different layers of the ionosphere under quiet geomagnetic conditions has the greatest influence on daytime ionospheric variations (Hargreaves, 1992; Rishbeth, 1998). Although the amount of incoming solar radiation varies throughout the year depending on local time, seasons, latitude, and longitude, ionospheric electrodynamics responds in accordance by altering the temperature, wind effect, and thermospheric neutral density composition (e.g., Adimula et al., 2016; Fejer et al., 1979; Forbes et al., 2000; Mendillo et al., 2005; Schunk & Nagy, 1978; Zhao et al., 2009). Earlier research has examined ionospheric variation over a single station and a data set of a few years or a part of the solar cycle. Few studies (e.g., Jethva et al., 2022; Rao, Chakraborty, et al., 2019) have analyzed TEC data for the full solar cycle but for a single station. Also, no previous study that we are aware of includes full solar cycle TEC data over geomagnetic conjugate low-latitude stations. Kalita et al. (2022) and Rao et al. (2013) are perhaps the only studies using TEC data for geomagnetic conjugate low-latitude stations. However, these studies were limited in scope, focusing on seasonal variations in TEC and hemispheric asymmetry in EIA strength. Furthermore, no previous research had included full solar cycle TEC data over geomagnetic conjugate low-latitude locations. The present paper is the first article in which the intrinsic periodicities in TEC at pairs of geomagnetic conjugate stations, including a specific scenario of land- and sea-locked GPS stations, are studied over the solar cycle-24 (years 2009–2017). It is possible understand the physical origin of ionospheric variability by examining short-, mid-, and long-term periodic changes in ionospheric indices. Using the Lomb Scargle Periodograms, Nayar et al. (2004) demonstrated periodicities of 13.5, 18, 27, 55, 155, 180, 365, and 475 days in low-latitude electron and ion temperature data from 1995 to 2000. According to Li et al. (2013), the amplitude of periodic fluctuations in the daily averaged TEC time series changes dramatically with solar activity and latitude. Ma et al. (2009) investigated the periodicities in globally averaged TEC from 1995 to 2008 using the wavelet technique, and their results reveal that the time-variable characteristics of 27-day, semi-annual, and annual components corresponded to wavelet scales of 20–40 days, 160–220 days,

and 330–420 days, respectively. Lean et al. (2011) analyzed the modeled global TEC time series from 1995 to 2010 and observed that the periodogram power near 182-day is equal in the northern and southern hemispheres. However, power near 365-day is substantially larger in the southern hemisphere. The annual oscillation is most noticeable in the southern hemisphere, with the greatest amplitude over mid-latitude in South American region (Lean et al., 2016). Lean et al. (2011) observed a strong presence of spectral power near 27-day in the solar EUV but a weak 27-day spectral peak in the TEC time series. Chandrasekhar et al. (2016) investigated the multi-fractal behaviour of TEC pertaining 27-day variations and its harmonics using IGS TEC data obtained from 27 stations in the latitude band 30°S–80°N along longitude sector 35–80°W for the low solar activity year 2008 and high solar activity year 2014. They reported that the 13.5-day variation could be influenced primarily by semi-lunar tidal effects, whereas the 9-day period could be influenced by day-to-day TEC variability. De Abreu et al. (2017) used wavelet analysis to determine small oscillations with periods of 1–10 days, 16–32 days, and 27–32 days in equatorial and low-latitude TEC related to planetary waves, semidiurnal tides, and solar rotation. Ionospheric variability is primarily influenced by changing solar EUV ionizing radiation (Schunk & Nagy, 2009), but lower atmosphere meteorology is also a factor (Immel et al., 2006; Rishbeth, 2006). The most significant components of the stratospheric equatorial circulation of zonal winds are the QBO of periods 22–34 months, characterized by alternate easterly and westerly phases in the zonal wind. The momentum flux supplied through Kelvin waves, Rossby-gravity waves (Holton & Lindzen, 1972), and gravity waves are considered to drive stratospheric quasi biannual oscillation, SQBO (Dunkerton, 1997). The ionospheric signatures of QBO were evident in the results of Chen (1992), who proposed that upward propagating waves primarily cause the day-to-day equatorial ionosphere anomaly region variability via the neutral wind dynamo effect (Lu et al., 2009; Neumann, 1990). Another possible factor is the relationship between solar and geomagnetic activity (Chanin et al., 1989; Kane, 2005). Tang et al. (2014) discovered SQBO-type periods with spectral peaks around 24- and 30-month in low-latitude TEC data from high and moderate solar activity years that is, 1999–2005. The QBO signals in the critical frequency of the F2 region (foF2), critical frequency of the E region (foE), the maximum height of the F region (hmF2) (Echer, 2007; Kane, 1995), and maximum electron density (Kurt et al., 2016) were also detected. Several hypothesis for ionospheric QBO have been proposed, including SQBO (Echer, 2007), solar activity (Berson & Kulkarni, 1968), the influence of the interplanetary magnetic field and geomagnetic activity (Kane, 1995; Maliniemi et al., 2016), and equatorial electrojet (Raja Rao & Joseph, 1971).

It is necessary to accurately predict the characteristics of the ionosphere's F2 region during various solar activity phases. The Community Coordinated Modeling Center (CCMC) made significant efforts to model the ionospheric parameters in this direction. (http://ccmc.gsfc.nasa.gov/modelweb/ionos/about_ionos.html). The Thermospheric and Ionospheric Electrodynamics General Circulation Model (TIE-GCM), which is driven by inputs from the magnetosphere, solar radiation, and Mesosphere and Lower Thermosphere (MLT) inputs from below 95 km, is one of the best options for studying the ionosphere feature (Richmond, 1992; Roble et al., 1988). Thus, in addition to the GPS TEC time series, we used the TIE-GCM TEC time series obtained for two pairs of geomagnetic conjugate stations. The northern low-latitude land-locked station Varanasi is the geomagnetically conjugate location to the southern low-latitude sea-locked station DGAR. Similarly, the northern low-latitude land-locked station LHAZ is the geomagnetically conjugate location to the southern low-latitude sea-locked station COCO Island. Also, station Varanasi is in the Gangetic plane, whereas LHAZ is in the Himalayan zone. Station DGAR and COCO Island; on the other hand, are in the central and eastern Indian Oceans, respectively. Using the TEC time series for the period 2009–2017 encompassing the solar cycle-24 from GPS and TIE-GCM, this work was carried out to determine how sea-locked versus land-locked lower atmospheric conditions, latitudinal location of stations, and hemispheric asymmetry affect TEC variability and the inherent periods of TEC trends, as well as understand the potential physical relationships for observed TEC periodicities. It is also intriguing to examine how the TIE-GCM displays the TEC periods. To the best of our knowledge, no studies have compared periodicities in TEC (GPS and TIE-GCM) time series of a solar cycle at geomagnetic conjugate low-latitude locations of specific cases of land-locked and sea-locked stations.

2. Data Set and Methods

This work examined TEC data from two pairs of geo-magnetically conjugate stations (see Figure 1) for the years 2009–2017. Among them, the Varanasi (25.31°N; 82.97°E; Mag. 16.57°N) and LHAZ (29.65°N; 91.10°E, Mag. 20.42°N) are northern low-latitude land-locked GPS stations, while DGAR (7.27°S; 72.37°E, Mag. 14.89°S) and COCO Island (12.18°S; 96.83°E; Mag. 21.35°S) are southern low-latitude sea-locked GPS stations. Out

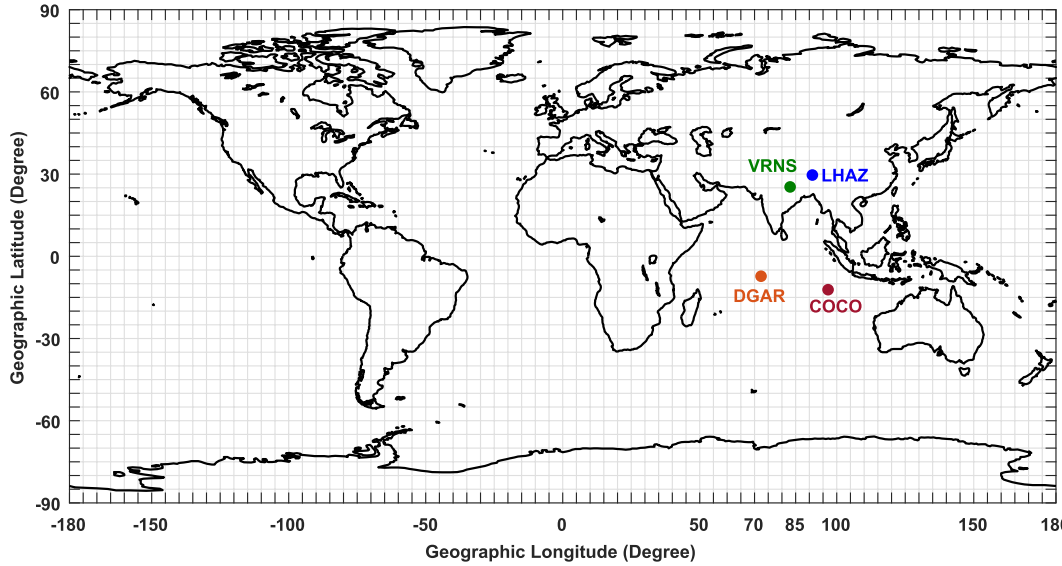

Figure 1. The geographical locations of the chosen GPS stations are shown. The northern land-locked station Varanasi (25.31°N; 82.97°E; Mag. 16.57°N) and the southern sea-locked station DGAR (7.27°S; 72.37°E; Mag. 14.89°S) are mutually the geo-magnetically conjugate locations. Similarly, the northern land-locked station LHAZ (29.65°N; 91.10°E; Mag. 20.42°N) and the southern sea-locked station COCO Island (12.18°S; 96.83°E; Mag. 21.35°S) are geo-magnetically conjugate locations of each other.

of four stations, LHAZ, DGAR, and COCO are IGS (International GNSS (Global Navigation Satellite System) Stations) stations, and their Receiver Independent Exchange (RINEX) formatted TEC data are available via the files transfer protocol using the link-garner.ucsd.edu. A registered user can download IGS TEC data through html or ftp access at Crustal Dynamics Data Information System (CDDIS) website: https://cddis.nasa.gov/archive/gnss/data. The software tool to process the RINEX formatted TEC data used in the present study could be found elsewhere (Seemala & Valladares, 2011). This software tool takes care of the satellite (b_s) and receiver (b_R) errors (accessible from ftp.uni-be/aiub/CODE) inherent to the un-differenced pseudo-range and carrier phase observations on L1 (1,575.42 MHz) and L2 (1,227.6 MHz) carrier frequencies during the post-processing of data to obtain corrected slant total electron content (STEC). The tool of Seemala and Valladares 2011 provides VTEC computed from the corrected STEC using the following equation (Birch et al., 2002).

$$\mathrm{VTEC} = {}^{(\mathrm{STEC} - [b_R + b_S])}/_{\mathrm{S}(\mathrm{E_l})} \tag{1}$$

$\mathrm{S}(\mathrm{E_l})$ is known as the obliquity factor or mapping function, and it is computed as a reciprocal function of the cosine of the solar zenith angle (χ). χ depends on the satellite's elevation angle $\mathrm{E_l}$ in degrees at the Ionospheric Pierce Point (IPP). According to the thin shell model (Mannucci et al., 1993), it is also affected by the mean Earth's radius and the ionospheric effective height h.

$$\mathrm{S}(\mathrm{E_l}) = \frac{1}{\mathrm{Cos}(\chi)} = \left\{1 - \left(\frac{R_E\,\mathrm{Cos}\ (\mathrm{E_l})}{R_E + h}\right)^2\right\}^{-1/2} \tag{2}$$

Mannucci et al. (1993) have proposed a two-dimensional thin shell model at 350 km ionospheric height to define the slant and vertical TEC mapping function. VTEC is abbreviated as TEC from now on.

TIE-GCM TEC data have been obtained from the CCMC website. We have obtained model data under the “Runs on Request" facility of CCMC from the advanced TIE-GCM version 2.0. The monthly data files were published on the CCMC website at the link-https://ccmc.gsfc.nasa.gov. The data are available at the “view request result” interface with run registration number sardar_rao_xxxxxx_IT_y. Here, x stands for the date of the model run, and y is the run number. The 3D time series of data for a given location could be created via a web interface. The height limitation set in the TIE-GCM simulation is 97–500 km. The main input parameters used are daily F10.7 solar indices, 81-day center-averaged F10.7 solar flux, the 3-hr Kp index, ionospheric electric fields at high

latitudes provided by the Heelis model (Heelis et al., 1982), and the Weimer model (Weimer, 2001), and diurnal and semi-diurnal migrating tides specified by the GSWM (Solomon et al., 2016). Thus, in the present analysis, we have used GPS-derived TEC and TIE-GCM TEC data for 2009–2017 over two pairs of geo-magnetically conjugate locations (Figure 1). The quiet time TEC time series were prepared by excluding data on days when the Dst index was less than −30 nT and solar flares of class *M* or more occurred.

In the present analysis, we have used two spectral techniques: the Lomb-Scargle periodogram (LSP) and wavelet coherence.

Lomb-Scargle periodogram-We have applied LSP to the time series of the daily mean data of F10.7 flux and Ap indices. We employed the daily data of noontime TEC values for the TEC time series. This spectral analysis technique helps to evaluate periodicities in unevenly sampled data (Horne & Baliunas, 1986). The variable (here F10.7, Ap, and TEC) or time can contain NaN values, which are treated as missing data and excluded from the spectrum computation. LSP evaluates the Lomb-Scargle power spectral density (PSD) up to a maximum frequency. If the signal is sampled atN non-NaN instants and Δt is the time difference between the first and the last of them, then PSD is returned at round (fmax/*f*min) points, where $f\text{min} = 1/(4 \times N \times \text{ts})$ is the smallest frequency at which PSD is computed and the average sample time is $\text{ts} = \Delta t/(\text{N} - 1)$. fmax defaults to $1/(2 \times \text{ts})$, which corresponds to the Nyquist frequency for uniformly sampled signals. A false alarm probability (fap) is a simple estimate of the significance of the height of a peak in the power spectrum.

Wavelet Coherence-The magnitude-squared wavelet coherence measures the correlation between two non-stationary real-valued signals of equal length (here TEC vs. F10.7 flux and TEC vs. Ap index) in the time-frequency plane. Thus, this method does not handle missing or NaN values. Therefore, we have used the 365-day smoothed data to overcome missing or NaN values errors while running the wavelet coherence code. The output of spectral coherence gives a wavelet coherence plot and cone of influence. Due to the inverse relationship between frequency and period, a plot that uses the sampling interval is the inverse of a plot that uses the sampling frequency. For areas where the coherence exceeds 0.5, plots that use the sampling frequency display arrows show the phase lag of TEC to F10.7/Ap. The direction of the arrows corresponds to the phase lag on the unit circle. For example, a vertical arrow indicates a π/2 or quarter-cycle phase lag. The corresponding lag in time depends on the duration of the cycle.

3. Analysis and Results

The solar cycle trends of TEC is presented in Section 3.1, and the inherent short- and mid-term periodicities in the TEC time series are discussed in Section 3.2.

3.1. Solar Hysteresis Effects in TEC

The solar cycle variation in TEC is presented by employing the 365-day-centered-running mean (McIntosh & Leamon, 2015) of daily F10.7 flux indices and noontime maximum TEC values from 2009 to 2018. We have fixed the noontime maximum TEC values at 09 UT±2 hr over Varanasi (VRNS) & DGAR and at 07 UT± 2 hr over LHAZ & COCO Island based on TEC contour plots of monthly mean TEC values (not shown here). Running means have been calculated based on these noontime maximum values. Missing data are handled with NaN values. For calculations in MATLAB, the kernel is selected to look at 365 elements, and then running sums are calculated. Running counts are also calculated to get the values of the number of days available in the specified data window, and running means are calculated. Figure 2 shows two broad peaks in the variation of F10.7 flux during solar cycle-24, the first occurring in January 2012 and the second in March 2014. Following the trends of F10.7 flux variation during the solar cycle, GPS and TIE-GCM TEC also showed double maxima during the solar cycle.

The TIE-GCM model flawlessly replicates the observed solar cycle with twin solar maximum peaks, as shown in Figure 2. It is seen from Figure 2 that the variation and peaks in the TIE-GCM follow the trends of solar flux variation. The first maximum in TIE-GCM is concurrent with the first maximum of F10.7 flux. However, the second maximum in TIE-GCM is found to be slightly shifted over Varanasi and COCO Island stations. It is considered that the local time for maximum noontime TEC varies with seasons (Rao, Chakraborty, et al., 2019; Sunda & Vyas, 2013) and that the TIE-GCM time slot for maximum noontime TEC may differ by *a* ±1 hr. For

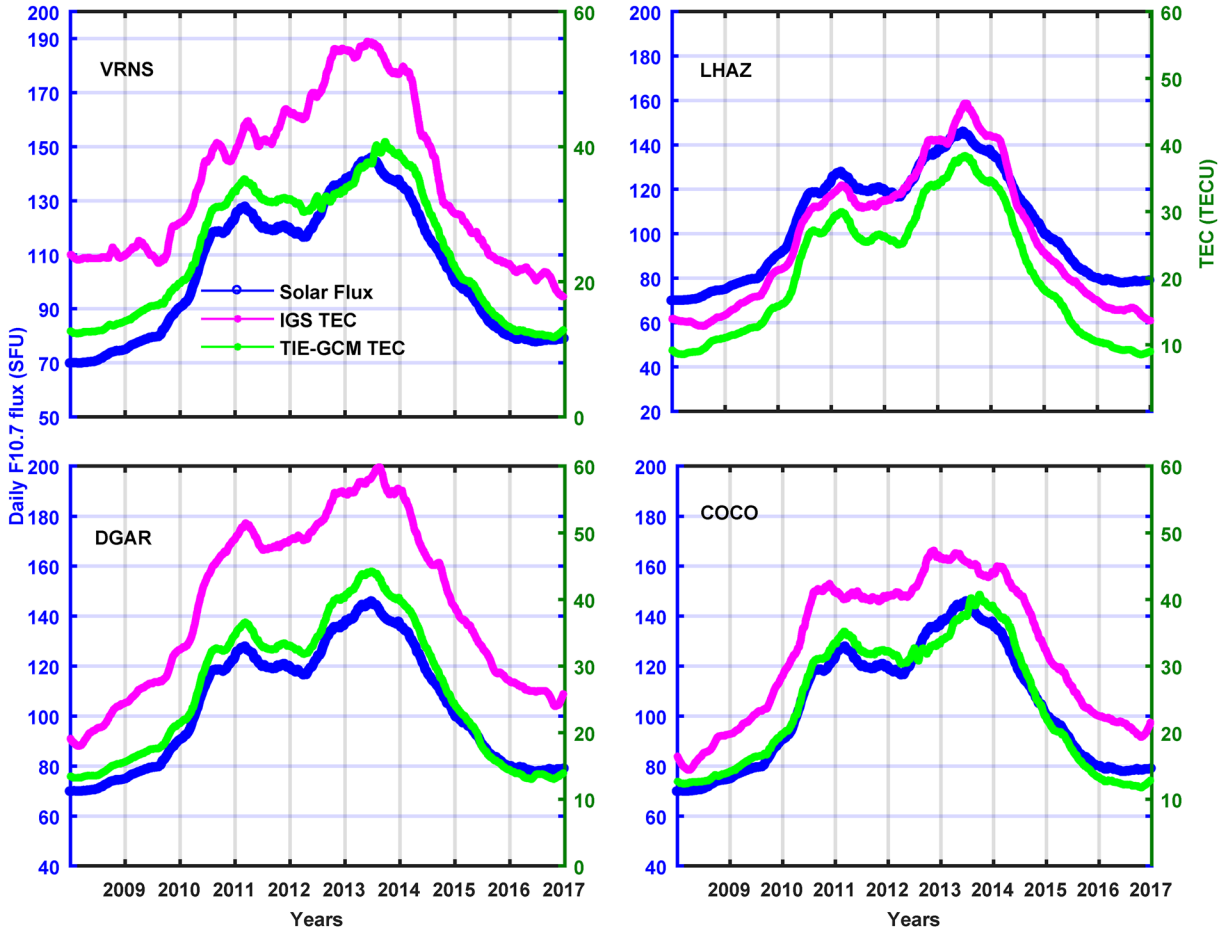

Figure 2. The solar cycle variation of the 365-day cantered running mean of F10.7 flux indices (blue curve), Global Positioning System (GPS) Total Electron Content (TEC; pink curve), and Thermosphere-Ionosphere-Electrodynamics General Circulation Model (TIE-GCM) TEC (green curve) is shown. The left ordinate gives the scale of F10.7 flux, and the right ordinate gives the scale of TEC.

timeslot uniformity, we have ignored this fact in the analysis. Thus, the observed shifting of the second maximum in the TIE-GCM for the F10.7 flux is considerable.

Another major observation from the solar cycle variation of solar flux and TEC is the gradient in TEC changes between the solar maximum year of 2014 and both start and end minima (years, 2009 and 2017). The F10.7 flux was changed from 2009 to 2014 (ascending phase) by 100% and from 2014 to 2017 (descending phase) by 87% of the solar cycle. Thus the ascending phase rate of change ($\frac{d\text{TEC}}{dt}$) was slower with greater changes in flux values, and descending phase time rate was faster with smaller changes in flux magnitude. The different gradient in TEC changes during ascending and descending phases exhibit the presence of solar hysteresis in a plot of TEC versus F10.7 flux, which is elaborated in Figure 3. Here, we used the data set of an almost complete solar cycle to examine the spurious trend of the hysteresis effect (e.g., Adler & Elias, 2008; Elias, 2014) based upon the suggestion of Danilov and Mikhailov (1999).

It can be seen from Figure 3 that the TEC has many values at the given F10.7 flux during the ascending and descending phases. A straight-line fit to the 12-month running mean of monthly mean F10.7 flux and TEC values shows a good correlation coefficient ($0.85 < R < 0.95$) during the ascending and descending phases of solar cycle-24. The correlation coefficient is more prominent during the descending phase than in the ascending phase. The high correlation coefficient between the two indices confirms the dominant role of solar flux in TEC variability at low-latitudes.

The slope of linear fit gives the TEC variation during both phases. The slope of the straight-line fit in GPS TEC variation relative to solar flux variation at Varanasi was determined to be ~0.28 and ~0.49 during the ascending

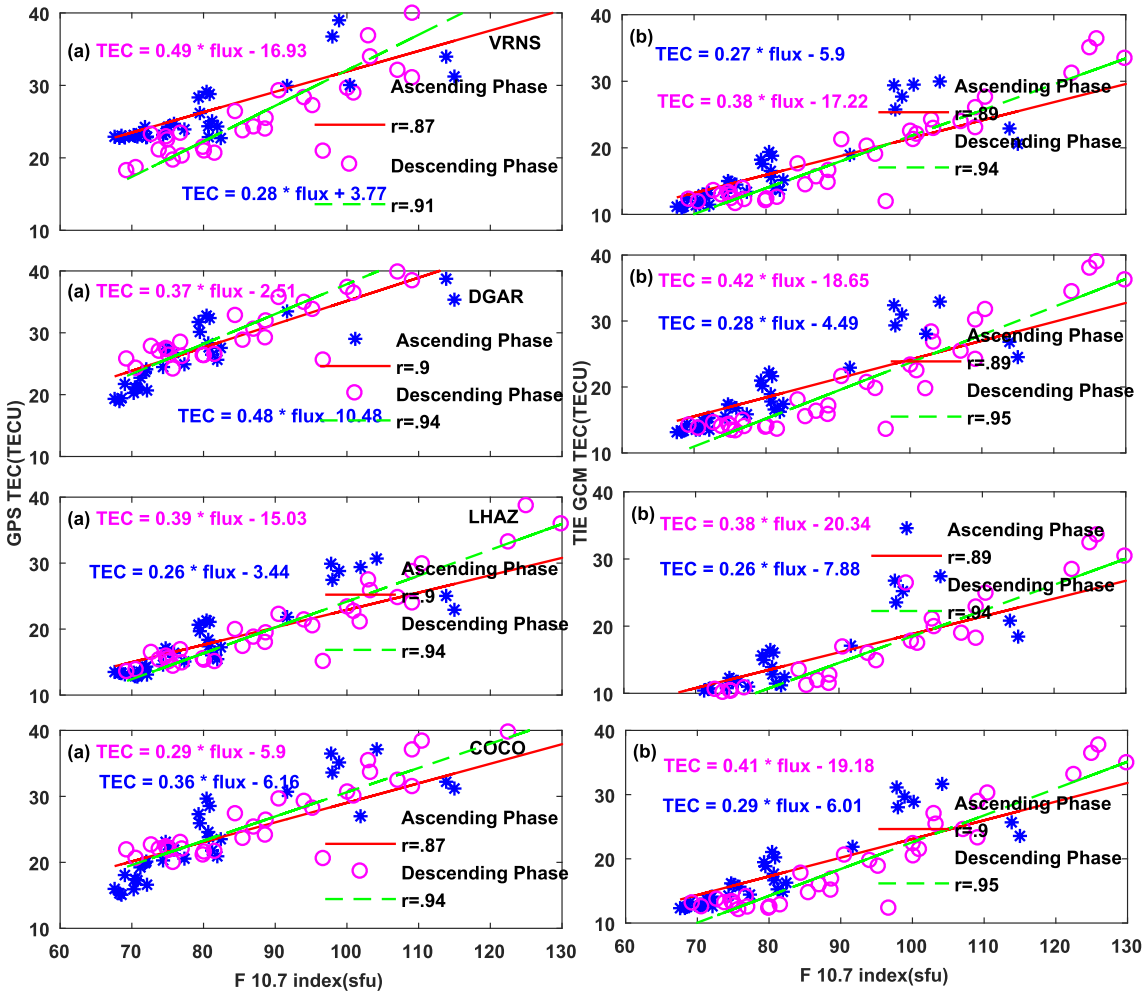

Figure 3. A straight-line fit to the 12-month running mean of monthly mean noon Global Positioning System (GPS)-Total Electron Content (TEC) values (left panel) and Thermosphere-Ionosphere-Electrodynamics General Circulation Model (TIE-GCM) TEC values (right panel) versus the F10.7 index are shown. The blue asterisk refers to TEC values during the inclining phase (2009–2014), and the magenta circle refers to TEC values during the declining phase (2015–2017) of the solar cycle-24. The regression fits are shown by solid lines, with red for the inclining phase and green for the declining phase of solar cycle-24. The seasonal dependency of solar hysteresis using monthly averaged data over the period 2009–2017 is presented in Figures 3.1–3.4 in the Supporting Information S1.

and descending phases of solar cycle-24, respectively. At COCO Island, it is found to be 0.36 and 0.29 during the ascending and descending phases of solar cycle-24, respectively. It is estimated to be 0.48 and 0.37 at DGAR during the ascending and descending solar cycle-24, respectively. At LHAZ, it is found to be 0.26 and 0.39 during the ascending and descending phases of solar cycle-24, respectively. Thus, the TEC versus flux correlation is reversed at sea-locked stations compared to land-locked stations. The hysteresis effect in TEC and solar flux could be associated with geomagnetic control of the solar cycle (Mikhailov & Mikhailov, 1995). The different TEC modulations relative to the solar flux at different stations shows the effect of local electrodynamics on geomagnetic activity.

The important outcome of the results is that the slope in TEC changes at both sea-locked stations during the ascending phase is more significant than in the descending phase. At land-locked stations, Varanasi and LHAZ, the slope in TEC trends is determined to be greater during the descending phase of the solar cycle. However, TIE-GCM TEC trends show a greater slope during the descending phase at all stations, and therefore, congruent behaviour in solar cycle variation is reflected. Also, TIE-GCM shows a clockwise hysteresis pattern when TIE-GCM TEC is plotted as a function of F10.7 flux. In contrast, GPS TEC hysteresis is clockwise at landlocked stations (Varanasi and LHAZ), and positive or negative hysteresis is found to be saturated in GPS TEC at the low solar activity side at sea-locked stations (DGAR and COCO). It is also observed from Figure 3 that the hysteresis effect is more pronounced at higher values of F10.7 flux, that is, around the solar cycle turning epoch. At this

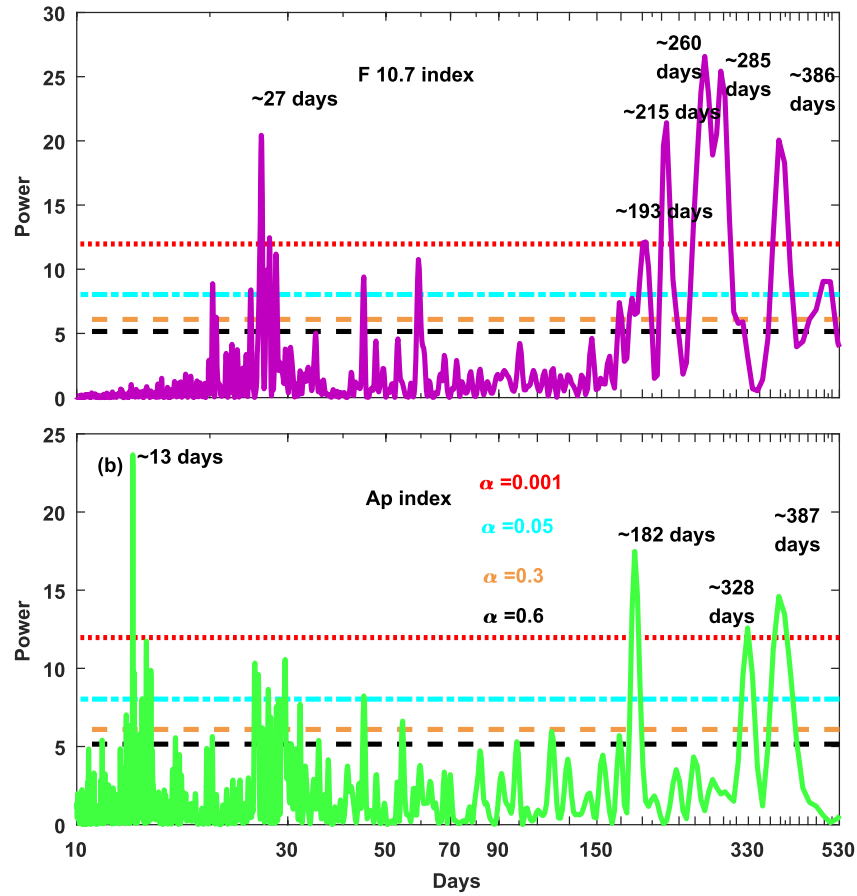

Figure 4. The periodicities inherent to the daily F10.7 indices (upper panel) and Ap indices (lower panel) on applying the Lomb-Scargle periodogram technique are shown.

period, the effect might be related to varying geomagnetic activity between the ascending and descending phases, inter-hemispheric plasma flow, and neutral wind changes (Hajra et al., 2016). As discussed earlier, the local time dependency of noontime TEC values during different seasons may be the reason for the time lag in shifting maxima (time-wise mismatching of peaks in flux and TEC). Another possible explanation for a lag in maximum occurrence relative to the solar flux peak might be the distinct hysteresis behaviour in GPS TEC. The local time dependency of hysteresis is a well-known characteristic (Chakraborty & Hajra, 2007). Section 4.1 of the discussion provides a detailed explanation of the findings related to the solar cycle patterns of TEC (Figures 2 and 3).

3.2. Lomb Scargle Periodogram Analysis

The Lomb Scargle periodogram technique (Scargle, 1982) is applied to F10.7 flux, Ap indices and TEC (GPS and TIE-GCM) time series of 2009–2017.

First, we have analyzed F10.7 flux and Ap index daily data for 2009–2017 to explore inherent periodicities in solar and geomagnetic activity. The LSP applied to the F10.7 flux and Ap index time series is given in Figure 4. To detect the inherent periods based on the ionosphere characteristics, we constructed a time series of TEC (GPS and TIE-GCM) noontime values for the period 2009–2017. The LSP applied to the TEC time series is shown in Figure 5. The observed periodicities are shown in Figures 4–5 are also presented in Table 1. The *X* marks show absent periodicity in the given time series (Table 1). The horizontal dashed lines shown in Lomb Scargle Periodogram figures are lines that show the level of significance of spectral peaks in terms of false alarm probability (fap). A fap is a simple estimate of the significance of the height of a peak in the power spectrum. The fap values are expressed as a number between 0 and 1. fap levels help to distinguish between significant and spurious peaks. The lower the fap for a given period, the more likely period is a significant period. Here, fap = 0.001 shows that peaks lie above this level are most significant. We only considered the periods that exist above the fap 0.05. The

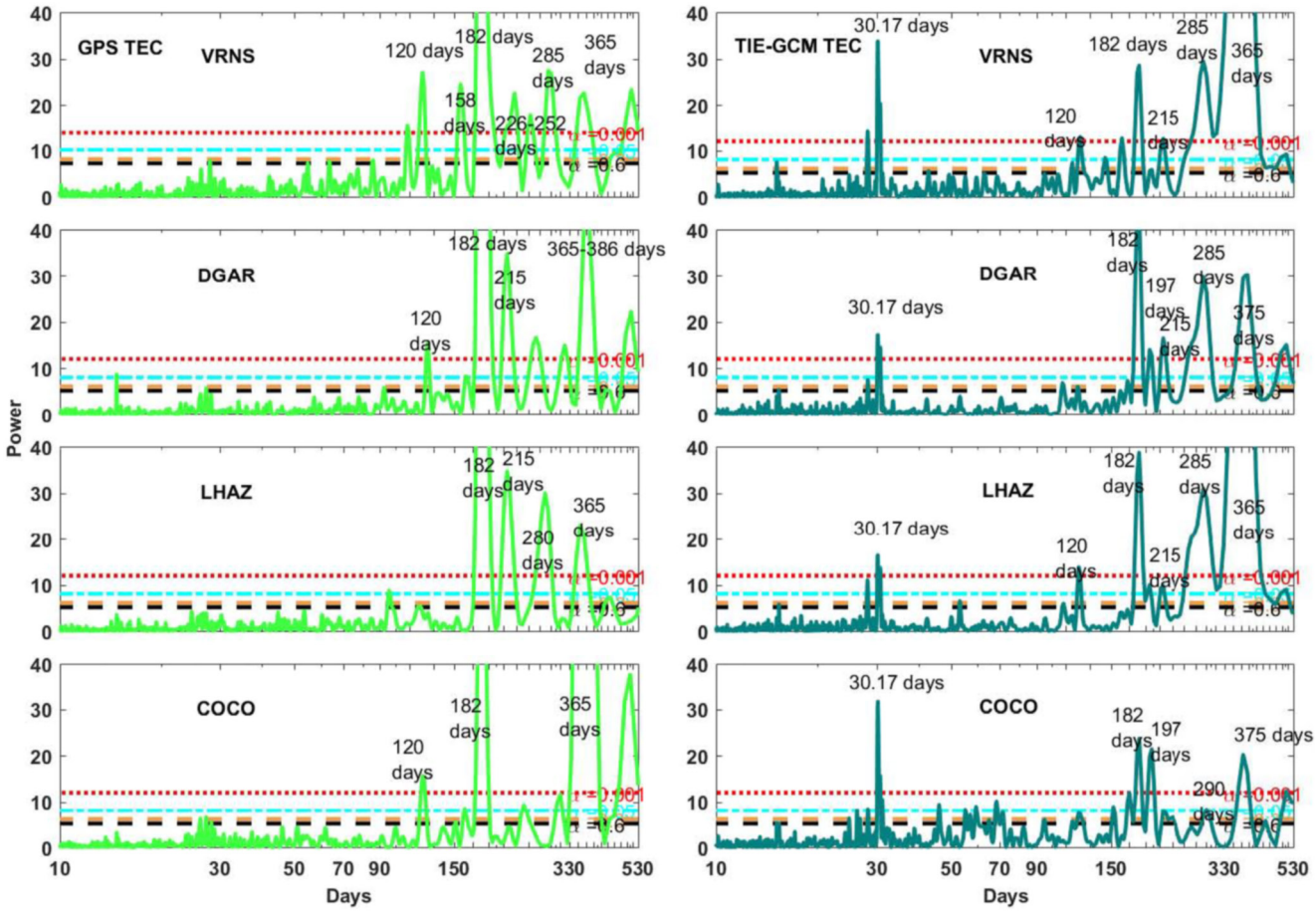

Figure 5. The periodicities inherent to the daily noontime maximum Global Positioning System (GPS)-Total Electron Content (TEC) (left panel) and Thermosphere-Ionosphere-Electrodynamics General Circulation Model (TIE-GCM) TEC (right panel) data on applying the Lomb-Scargle periodogram technique are shown.

periodicities that lie near and above $\alpha = 0.001$ are shown in red; the periodicities that lie near and above $\alpha = 0.05$ are shown in green; and the periodicities that lie near and above $\alpha = 0.3$ are shown in gray. In the following, we look over each periodicity detected in the time series of the TEC, Ap index, and F10.7 flux.

Solar Rotation — An LSP shows a significant presence of a solar rotation period (~27-day) in the F10.7 flux time series. The other less significant periods of 20.29-day, 44.50-day, and 59.50-day in F10.7 index are also observed with power amplitude <10 (0.001 > fsp > 0.05). In the Ap index data series, 13.5-day with power >15 and 14.4-day, 25.5-day, 27-day, 29-day, 44.5-day periods with power <10 were detected. The first harmonic of the solar rotation period (13.5-day) is strongly present in AP indices with sidebands of 25–29-day, although the solar rotation period itself is less significant. A solar rotation period (~27-day) and first harmonic period (13.5-day) did not found in the GPS TEC time series. However, the TIE-GCM time series at all stations showed the sidebands of the solar rotation period (about 30–31 days).

The 27-day and 13.5-day periodicities are reported to be observed in the solar wind, geomagnetic activity, interplanetary magnetic field, and ionospheric parameters (Donelly & Puga, 1990; Kane, 2003; Nayar et al., 2001, 2002; Zięba et al., 2001, and references therein). The intermittent short-term periodicities between 26- and 32-day in solar and geomagnetic data are consistent with Bai and Sturrock, 1987. According to Kane (2002), these peaks in F10.7 and Ap indices (26–32 days) can often deviate considerably from the solar rotation period of 27-day. Thus, the 25–30 days range could be considered a solar rotation period band.

A 13.5-day period observed in the Ap index is the harmonic of a 27-day periodicity, which has a relationship either with the fast Sun-oriented wind streams separated 180° in Sun-oriented longitude or with two dynamic areas isolated by 180° (Mursula & Zieger, 1996). de Gonzalez et al. (1993) relate a 13.5-day period in the Ap

Table 1
The Periodicities Exists in F10.7 Flux, Ap Indices and TEC (GPS and TIE-GCM) Using LSP Technique Are Given

Periodicities in daily noontime data										
	Stations		BHU		LHAZ		DGAR		COCO	
Parameters	F10.7	Ap	GPS	TIE-GCM	GPS	TIE-GCM	GPS	TIE-GCM	GPS	TIE-GCM
Periodicities										
27 Days	27	13, 25-29	X	28, 30	X	28, 30	X	28,30	X	26,30
120 Days			120	120	X	121	125	X	120	X
182 Days	193	182	182	182	182	182	182	182, 195-198	182	182, 195-198
215	215	X	215, 226	215	215	215	215	215	X	215
285 Days	260,285	X	285	285	280	285	X	285	X	291
365 Days	386	328,387	365	365–375	355–365	365–375	375	385	375	375
Periodicities in 365 days smoothed running mean data										
505 Days	505	X	505	505 (fap < 0.001)	505 < fap 0.3		504	505	505	505
597 Days	597	657	597	597	597		597	597	597	597
730	730		730	730	730		730	730	730	730
775	773	821	773	773	773		773	773	X	773
930	939		939 (≤0.001)	X	939 (fap = 0.001)		X	939 (≤0.001)	X	939

index with a complex interplanetary magnetic field division structure. The TIE-GCM TEC shows a solar rotation period of ~28–31 days (peak ~30.17-day) which is not seen in the GPS TEC. Thus, TIE-GCM shows a discrepancy in the appearance of the solar rotation period.

Semi-annual Oscillation- It is seen from Figure 4 that the spectral peak showing semi-annual oscillation occurred strictly at 182-day in the Ap indices, GPS TEC, and TIE-GCM TEC time series but at 193-day in the F10.7 indices. An extensive analysis of a semi-annual oscillation in different geomagnetic activity parameters could be found elsewhere (Lockwood et al., 2020; Russel & McPherron, 1973). The semi-annual component in TEC may result from the interaction of solar zenith distance, atmospheric circulation over the high-latitude zone, and the changing proportion of O/N2 (Fuller-Rowell, 1998). According to Russell (1971), the semi-annual (182-day) and seasonal components in geomagnetic activity are also linked with the Earth's translational movement (solstices), the inter-hemispheric symmetry (equinoxes), and the observational frame of reference. Concerning semi-annual periodicity in F10.7 flux, we bring the results of Chakrabarty et al. (2012), wherein they used the same LSP technique and found no stable and consistent phase relationship between semi-annual oscillations in EUV/SFU and TEC. However, they computed a 182-day period in the EUV/SFU time series of 2005–2009, but with significantly less spectral power and below a significant level. It can be seen from Figure 5 that the height of the spectral power of semi-annual peaks in the GPS TEC time series is almost the same at land-locked and sea-locked stations. Thus, it can be said that the semi-annual oscillations in GPS TEC have equal strength at northern and southern hemispheric stations and are not affected by the lower atmospheric conditions (land vs. sea). However, the height of spectral power in the TIE-GCM time series is unequal at all stations and shows latitudinal as well as longitudinal biases. The height of 182-day in TIE-GCM is significantly higher at DGAR and LHAZ compared to VRNS and COCO.

Annual Oscillation- It is noted from Table-1 that the period of ~365-day is determined to be present in the F10.7 flux, Ap index, and TEC (GPS and TIE-GCM) time series. The peak of annual periodicity is shown in the F10.7 flux data at 386-day and the Ap index at 328- and 386-day. The periodogram also noted that the amplitude of the semi-annual oscillation is fixed at 182-day, whereas the amplitude of the annual oscillation evolved from 355-day to 390-day. A variation of ±25 days in the annual component of the TEC time series has also been reported by Lean et al. (2011). In the case of the F10.7 and Ap Index, the annual LSP spectral peak is determined to be 386-day. The presence of an annual component is also evident in TEC, wherein larger TEC values during the December solstice are, on average, more extensive (by about 50%) than during the June solstice (Codrescu et al., 1999; Jee et al., 2004). As we discussed above, the power of the 182-day peak is almost equal in the GPS TEC time series of the northern and southern stations. In the case of the annual component, a hemispheric asymmetry is noted. The

power near 365-day is more than twice as high in the GPS TEC time series of the southern hemispheric stations compared to the northern hemispheric stations. This result is also true for the global TEC, as Lean et al. (2016) reported that the amplitude of the hemispheric averaged annual oscillation in the southern hemisphere dominates over the northern hemisphere. The TIE-GCM TEC time series shows 365-day peak strength that is exactly the opposite. The height of the 365-day spectral peaks of TIE-GCM appeared larger at northern stations than at southern stations. Thus, TIE-GCM can replicate semi-annual and annual components, but differences in the strength of peaks are still noted. Titheridge and Buonsanto (1983) suggested that, for TEC, the annual anomaly predominates over the seasonal anomaly in both the northern and southern hemispheres. Observations from the Hinotori satellite and the Sheffield University Plasmasphere Ionosphere Model (SUPIM) over low-latitudes showed that the global average of topside ionosphere electron density at the December solstice remains about 100% higher than that at the June solstice, compared to the 6% solar flux difference due to changes in Sun-Earth distance.

Inter-annual Components- In the periodogram, we identified the 280-day periodicity as an inter-annual component. It is seen from Figure 4 that the inter-annual period appears in the F10.7 index data at 285-day but not in the Ap index data. The spectral analysis showed the presence of a 280-day period in the GPS TEC time series at northern low-latitude stations but not at southern low-latitude stations. Contrary to this, TIE-GCM showed the presence of 280-day in TEC at both northern and southern low-latitude stations. In the TIE-GCM time series, the least spectral power of 280-day is obtained at COCO Island. It is also noted from Figure 5 that the spectral height of the 280-day periodicity in GPS TEC is greater than the 365-day periodicity at northern stations. Contrary to the GPS TEC time series, the height of the spectral peak in the TIE-GCM time series is greater for 365-day compared to 280-day at all stations except DGAR. At DGAR, both peaks have nearly equal spectral power. TIE-GCM shows a significant inter-annual component of 280-day at northern and southern low-latitude stations. The presence of an inter-annual component in TIE-GCM TEC at northern low-latitudes is consistent with the presence of a seasonal component. TIE-GCM, contrary to observations, exhibits seasonal components at southern low-latitudes. Thus, the TIE-GCM simulates the seasonal component of the 280-day in the model TEC at southern low-latitudes. TIE-GCM may not account for solar flux, hemispheric and regional dependence of the seasonal anomaly of TEC. As a result, the model presumes a seasonal component in TEC at northern as well as southern low-latitudes. The explanation for TIE-GCM dissimulation of the seasonal component in TEC is discussed separately later in Section 4.2.

Quasi-Biannual Oscillation (QBO) - To find QBO oscillations accurately without spurious periods in the data time series, we have used 365-days-smoothed-running mean data to obtain periodicities in TEC (Figures 6-7, Table 1). Some QBO periodicities that are not seen as distinct in daily data can be distinctly identified from the time series of 365-days-smoothed-running mean data.

In the F10.7 data series, we find 597- and 730-day periods with power amplitudes greater than 15. The 626-day and 820-day periods with powers less than 10 appeared in the AP index data series. The 505-day periodicity is observed in the GPS and TIE-GCM TEC time series at all stations. However, it appeared below fap = 0.3 in GPS TEC at LHAZ, which is well below the significant level. It is essential to mention that this period is also observed in F10.7 flux index but not in the Ap Index.

It is seen from the periodogram shown in Figure 7 that the period of 597-day (20-month, 1.63-year) is present in GPS as well as TIE-GCM TEC at all four stations. The 597-day oscillation is also visible in the F10.7 flux. The 730-day (2-year) period observed in the F10.7 flux is also evident in the GPS and TIE-GCM TEC at all stations. Surprisingly, the spectral peak of 773-day periods was observed at all of the selected stations except GPS TEC at COCO Island. A careful examination of spectral peaks for 730- and 773-day reveals that both periods exist within a single spectral peak distinguished by a small excursion at 773-day. However, at COCO Island, the period of 773-day is merged with a significant spectral peak of 730-day. Also, the 939-day (31-month) period is present in GPS TEC at all stations but is observed to be highly significant at COCO Island. The 939-day period is not obtained in the TIE-GCM TEC time series at any stations. A detailed account of the possible physical cause of QBO oscillation in TEC is given in Section 4.3.

4. Discussion

4.1. Modulations and Solar Hysteresis in TEC Solar Cycle Variation

The time interval between two successive maxima in F10.7 flux (or TEC) is known as the Gnevyshev gap, and it is roughly two years long (Krainev et al., 1997; Storini, 1997). The observation of double maxima in TEC

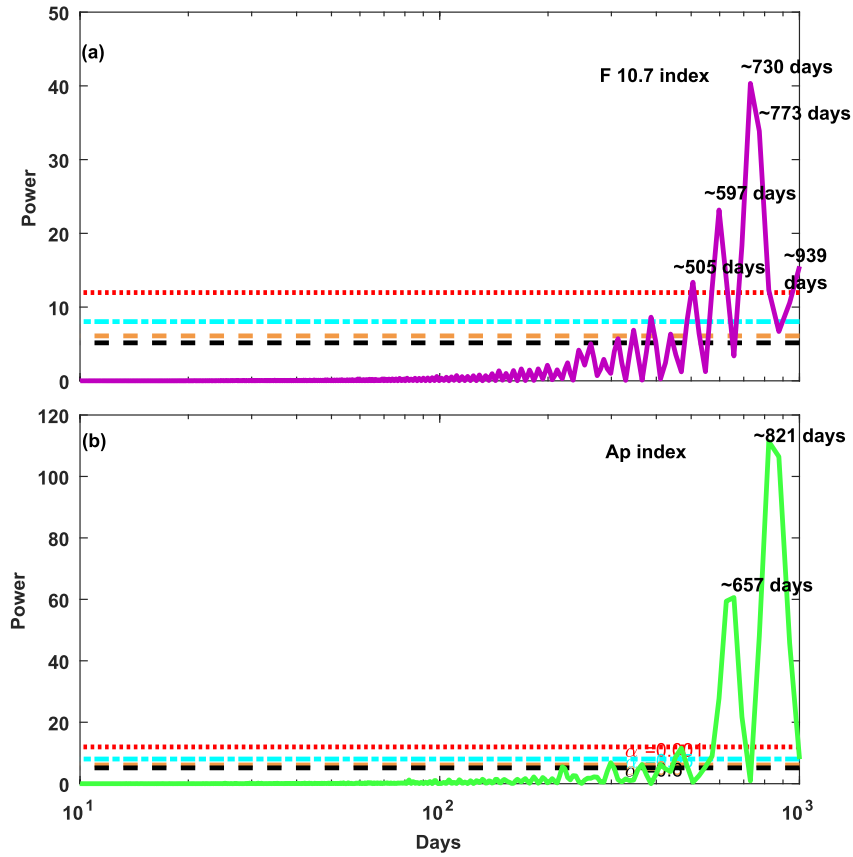

Figure 6. The Lomb-Scargle periodogram for the 365-day center-running mean F10.7 (upper panel) and Ap (lower panel) indices of the period 2009–2017 is shown.

(Figure 2) during the solar cycle is consistent with Ozguc et al. (2008) and Kane (2010), who found double maxima in foF2. The appearance of double maxima during the solar cycle is a physical phenomenon that has also been observed in accompanying proxies (Gnevyshev, 1963; Kane, 2009, 2010). The double peaks in the TEC profile over a solar cycle are obvious because trends and variabilities in the ionosphere are highly correlated with variations in solar flux/sunspot number (Rao, Sharma, & Pandey, 2019). According to Gnevyshev (1967), the appearance of double maxima during the solar cycle is due to the superposition of northern and southern sunspot maxima. The well-known butterfly feature of sunspots is a superposition of the changing relative importance of the two consecutive maxima in both solar hemispheres. Thus, we see double peaks in latitudinal averaged sunspots over a solar cycle. Gnevyshev's theory could not be generalized because double peaks are not a common feature during all solar cycles and are sometimes observed in sunspot data from a single hemisphere (Norton & Gallagher, 2010).

Recent advancement has been made to develop a standard theory which explains the peculiar appearance of the Gnevyshev gap in the solar parameters and their proxies. In this regard, the latest model of Karak et al. (2018), based upon the kinematic axisymmetric Babcock–Leighton dynamo model, shows that the fluctuations in the solar polar field are responsible for producing these spikes and double peaks. When the polar field sets, large negative fluctuations in the Babcock–Leighton process can immediately diminish the net polar field. As these fluctuations in the polar field are propagated to the new toroidal field, they can enable double maxima in the subsequent solar cycle (Karak et al., 2018). Their explanation based on the theoretical model is also supported by polar field observations and results presented by Cameron et al. (2013) and Kitchatinov et al. (2018). Karak's theory also justifies the presence of multiple peaks and dips in the solar cycle variation of the solar parameters. For example, Figure 2 shows a spike during November 2011, the first peak during January 2012, and the biggest one during March 2014 in F10.7 flux, with a dip during January 2013. A similar variation in TEC is seen during the solar cycle. TEC modulations in the solar cycle trend of TEC are depicted over Varanasi compared to the other

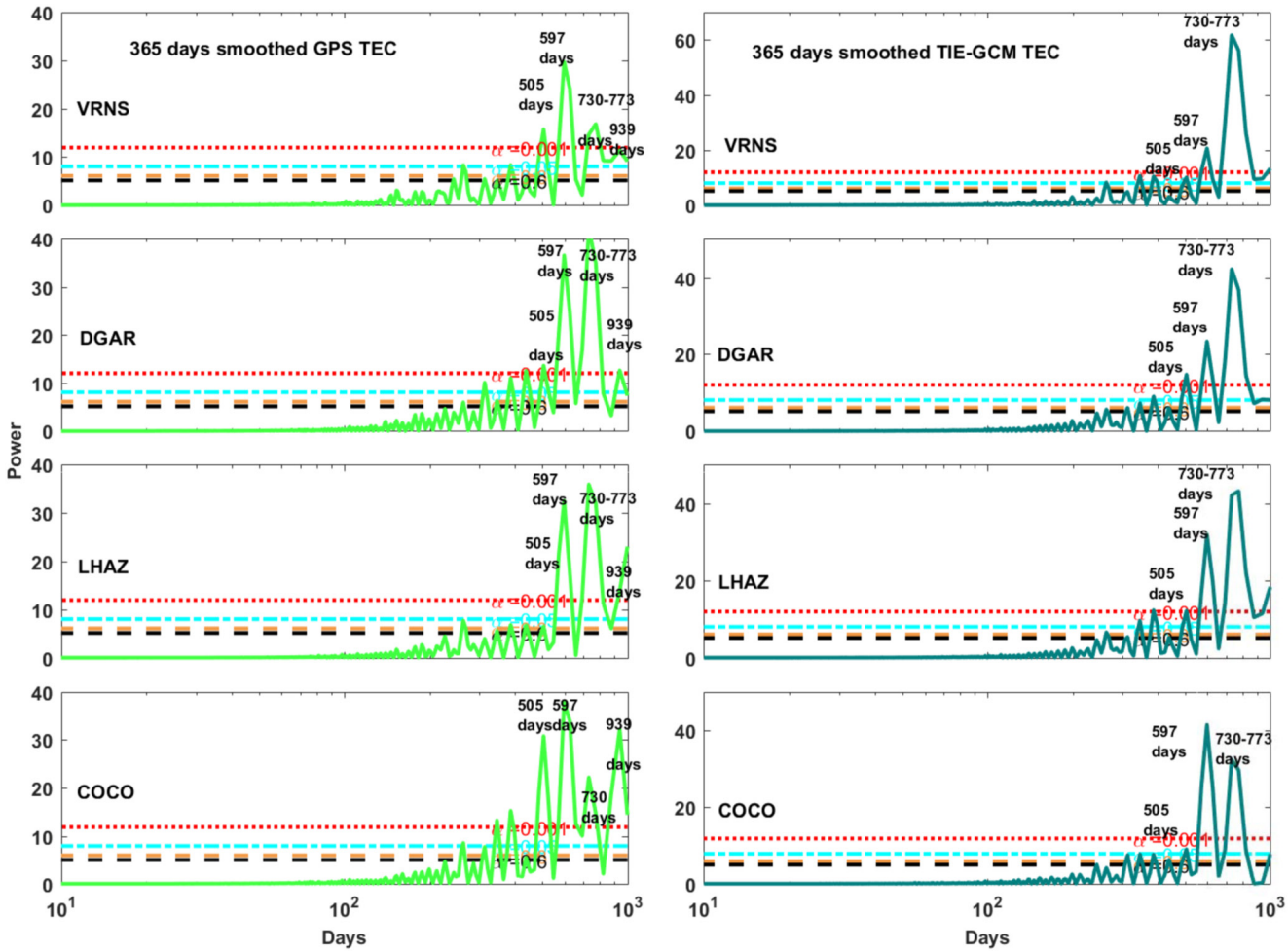

Figure 7. The Lomb-Scargle periodogram for the 365-day center-running mean Global Positioning System (GPS)-Total Electron Content (TEC) data (left panel) and Thermosphere-Ionosphere-Electrodynamics General Circulation Model (TIE-GCM) data (right panel) of the period 2009–2017 is shown.

three stations. Out of four stations, Varanasi, DGAR and COCO Island are located near the EIA crest, and also DGAR and COCO Island are sea-locked stations. Thus, compared to EIA crest stations DGAR and COCO Island, the modulated TEC trends over Varanasi may be related to the local electrodynamics of the northern EIA crest over the land-locked stations. The observed inter-hemispheric asymmetry is supported by the simulation results of Lin et al. (2005), which showed that the strong EIA inter-hemispheric asymmetry was related to the strong strengthening in the northern EIA crest due to the strengthened northward trans-equatorial wind perturbation. Also, the magnitude of peaks is greater at EIA stations (Varanasi, DGAR, and COCO) which show an additional effect of equatorial electrojet, EEJ (Rao et al., 2013).

The modulations in TEC variation (Figure 2), particularly at EIA stations, may arise due to the EEJ. It is because the day-to-day neutral wind effect is sorted out in the smoothed data. At low-latitudes, the TEC variability is highly influenced by ExB dynamics, where B is highly sensitive to hysteresis. The hysteresis effect in geomagnetic activity causes asymmetry in ionospheric electron density (here, TEC) between the ascending and descending phases of the solar cycle at an equal level of the solar index (Appleton & Piggott, 1955; Ikubanni et al., 2019). It is essential to mention that the different solar indices (F10.7, EUV, and sunspot number) also have a mutual inherent hysteresis effect (Kane, 2005). It is suggested by Rao and Rao (1969) that the more significant occurrence of geomagnetic activity during the descending phase of solar activity may be the key factor in the hysteresis effect. Huang and Jeng (1976) also reported that solar magnetic activity lags sunspot activity by about two years, leading to an asymmetry in the frequency or intensity of magnetic activity between two phases. Also, the nature of the hysteresis effect is variable and is a consequence of both meteorological influence and solar wind conditions

(Ozguc et al., 2008). TEC variability's local time and seasonal dependency during different phases of the solar cycle and their connection with hysteresis effects have been well reported (Ouattara & Amory-Mazaudier, 2012). We have also presented month-wise hysteresis plots (see Figures 3.1–3.4 in the Supporting Information S1) for TEC versus F10.7 flux for 2009–2017. It can be seen from these figures that the profile of hysteresis curves is different for different months. Chakraborty and Hajra (2008) interpreted the hysteresis in TEC as related to the cumulative effects of geomagnetic disturbances during the descending phase that may produce changes in neutral composition, temperature, and thermospheric wind pattern.

Thus, the results of solar cycle trends in GPS and TIE-GCM TEC over chosen land-locked and sea-locked stations could be summarized as follows: During solar cycle-24, the double hump structure with Gnevyshev gap is visible in F10.7 flux and TEC variation. A gradient in the TEC trend during the solar cycle shows a slower rate during the ascending phase and a faster rate during the descending phase. A solar hysteresis is observed in the solar cycle trends of GPS and TIE-GCM TEC. The hysteresis effect is visible at a higher flux value, that is, at the turning point between ascending and descending phases. Also, the profile of solar hysteresis is observed to be affected by seasons, local time, and latitudes. The slope of the GPS TEC versus F10.7 flux hysteresis curve is observed to be greater during the descending phase compared to the ascending phase at northern low-latitudes. At southern low-latitude stations, the slope of the hysteresis curve is observed to be greater during the ascending phase than during the descending phase. The slope of the TIE-GCM TEC versus F10.7 flux hysteresis curve is greater during the descending phase compared to the ascending phase at northern and southern low-latitude stations. At the northern low-latitude, hysteresis is clockwise, while at the southern low-latitude, it is either clockwise or counter clockwise.

4.2. Dissimulation of Inter-Annual Components by TIE-GCM

TEC variability is greatly influenced by short-, mid-, and day-to-day oscillations in addition to solar cycle variance. Rishbeth and Mendillo (2001) investigated solar radiation, geomagnetic disturbances, meteorological sources from lower atmospheric layers, and electrodynamics to account for such fluctuation. These parameters might be identified in the TEC data set using periodogram analysis. In several research, the periodicities of the 1-day, 27-day, semi-annual, and annual cycle in TEC data have been examined (Lean et al., 2011; Li et al., 2013; Guo et al., 2015; Forbes et al., 2018). The observed periodicities in TEC and TIE-GCM efficacy to replicate the observed periodicities are discussed below.

The most visible component in the GPS TEC time series is a periodic pattern with periods of $365.25/n$ days ($n = 1, 2, 3, n$). Different harmonics of annual components could be identified by a periodicity of 365, 182, 90, etc. days in the spectral analysis. During solar cycle-24, LSP analysis revealed the presence of a spectral peak at 182- and 365-day in GPS and TIE-GCM TEC time series at northern and southern low-latitude stations. These results are consistent with observations of semi-annual oscillation (Mansilla et al., 2005) and annual oscillation in NmF2/TEC (Shim, 2009).

The inter-annual component ~280-day corresponds to $\sim(\frac{2n+1}{4})$ 365.25 days, $n = 1$ could be considered seasonal component. The presence of 280-day in the GPS TEC time series at northern low-latitude stations and its absence at southern low-latitude stations confirms that the ionospheric winter anomaly does not exist across the southern hemisphere (Huo et al., 2009; Tsai et al., 2001). The winter anomaly has been found to be present in foF2 throughout the solar cycle and to vary in TEC depending on other factors such as solar flux and EEJ in the northern hemisphere (Lee et al., 2011; Rao et al., 2013; Yasyukevich et al., 2018). However, the TIE-GCM appears to have an inter-annual component (280 days) at southern low-latitude stations in the current LSP analysis, which implies that, contrary to previous findings, the TIE-GCM assumes the seasonal anomaly characteristic at southern low-latitudes. This could be the case because the TIE-GCM ignores the fact that the seasonal anomalous feature in TEC depends on several other factors and assumes a single mechanism is responsible for semi-annual, seasonal, and annual TEC oscillations. Because of this, the chemistry in TIE-GCM could not capture the crucial aspect of seasonal anomaly, as we will detail below.

Ionospheric plasma density losses are significantly due to the recombination of NO^+ and O^{+2}, which are created by the charge exchange of O+ with N_2 and O_2 (Volland, 1995). Further, the lower atmospheric pumping (e.g., Forbes, 1996; Goncharenko et al., 2010) via eddy diffusion can cause vertical mixing of neutrals that affect the local O/N_2 ratio. The TIE-GCM has a vertical grid with pressure surfaces extending from about 97 km to 500–800 km, depending on solar activity. The major neutral species in the TIE-GCM are N_2, O_2, and O. TIE-GCM version 2.0 includes O+ ions and assumes steady-state electron density chemistry. TIE-GCM used the

Weimer electric potential and precipitation models (Emery et al., 2008). Daily and 81-day averaged F10.7 were used to specify the solar EUV flux following the EUV flux model for aeronomic calculations, EUVAC (Richards et al., 1994). The neutral temperature at the lower boundary of TIE-GCM is fixed at 181 K with a constant density. Both migrating and non-migrating tides were included in the TIE-GCM through the specification of the altitude of the bottom pressure level as specified by the Global Scale Wave Model, GSWM (Hagan & Forbes, 2002). Since the tides are partly a result of solar EUV forcing, seasonal and local time variations exist within the GSWM. The uncertainty in internal model parameters causes differences between models, such as eddy diffusion. Eddy diffusion coefficients also have seasonal dependencies (Garcia & Solomon, 1985; Khattatov et al., 1997) that affect thermospheric neutral density and composition (Pilinski & Crowley, 2015; Qian et al., 2009). In a standard TIE-GCM, a constant eddy diffusion coefficient ∼125 m^2/s with respect to the day of the year is applied at the model lower boundary, fixed at 97 km. At this altitude, the notable species O_2 and N_2 mass mixing ratios are prescribed as 0.22 and 0.78, respectively. At the lower boundary, the vertical gradient of atomic oxygen (O) number density is specified as zero.

Therefore, O is effectively lost from the lower boundary of the model. Increasing eddy diffusion accelerates downward transport and removal of O, thereby decreasing O in the model. The TIE-GCM has simulated neutral density using the default constant eddy diffusion but failed to replicate the annual and semi-annual variation (Qian & Solomon, 2012). In the upgraded TIE-GCM version 2.0, the variable eddy diffusion was imposed at the model's lower boundary. As a result, annual or semi-annual variations in neural density were captured, which agree with the current observations and also with the findings of Qian et al. (2013). Eddy diffusion affects neutral density primarily by changing the thermospheric composition. Eddy diffusion transports atomic oxygen downward, against the mixing ratio gradient, from the lower thermosphere into the mesopause region, where it is annihilated by three-body recombination and hence decreases the O/N_2 in the thermosphere.

Qian et al. (2013) demonstrated that eddy diffusion changes the composition of the thermosphere and thus influences neutral density. The imposition of variable eddy diffusion causes the TIE-GCM O/N_2 to exhibit a semi-annual/annual variation. Using the variable eddy diffusion at the TIE-GCM lower boundary, Qian et al. (2013) also found features of a semi-annual and annual anomaly in NmF2 (or TEC) of the EIA region, which were consistent with the ionosonde observations. Thus, the TIE-GCM improvements in version 2.0 with variable eddy diffusion make composition changes in the daytime ionosphere more balanced, which increases the predictability of semi-annual/annual variation in O/N_2 and hence in electron density (here TEC). In other words, production rates are set approximately proportional to the atomic oxygen density, and chemical recombination loss rates are set approximately proportional to the molecular density, primarily N_2 and O_2 in the F region.

Even though the model includes the seasonally varying eddy diffusion, TIE-GCM version 2.0 still dissimulates a seasonal component (∼280-day), which is not compatible with the observations from southern low-latitudes. It is because seasonal variation (changes in electron density from summer to winter) is complicated owing to solar flux (Mikhailov & Perrone, 2014; Rao, Chakraborty, et al., 2019), regional (Huo et al., 2009; Yasyukevich et al., 2018; Zhao et al., 2007), and altitude dependency (Liu et al., 2007; Mikhailov & Perrone 2014; Su et al., 1998; Torr & Torr, 1973; Zhao et al., 2005). These factors were not taken care of in TIE-GCM version 2.0. The TIE-GCM version 2.0 improvements to account for seasonal variation of O/N_2 by imposing variable eddy diffusion do not account for the winter-to-summer variation of TEC (Maute, 2017). In this context, Yasyukevich et al. (2018) revealed the disagreement between the winter anomaly intensity in O/N_2 and TEC for their longitudinal oscillations in the northern hemisphere with the level of solar activity. The TIE-GCM version 2.0 includes O+ ion. Depending on the temperature, two essential reactions, $O^+ + N_2 \rightarrow NO^+ + N$ and $O^+ + O_2 \rightarrow O_2^+ + O$, may play different roles in the formation of the seasonal anomaly (Mikhailov & Perrone, 2014). This may be a possible reason whereby TIE-GCM predicts a seasonal component in the TEC time series at DGAR and COCO. In light of above, it may be said that the TIE-GCM assumes the seasonal component as a result of the application of seasonally varying eddy diffusion in TIE-GCM version 2.0 to account for seasonal fluctuation of O/N2. It is because the Rishbeth theory (Rishbeth et al., 1978) could not be fully applied to explain the latest results of the TEC winter anomaly (Mikhailov & Perrone, 2014; Rao, Chakraborty, et al., 2019; Yasyukevich et al., 2018).

4.3. Physical Process Causing TEC QBO (Spectral Coherence Analysis)

The tropospheric and mesospheric QBO's upward propagation, solar activity, and geomagnetic activity are thought to be the three primary causes of the ionospheric QBO, respectively. Additionally, the relevance of

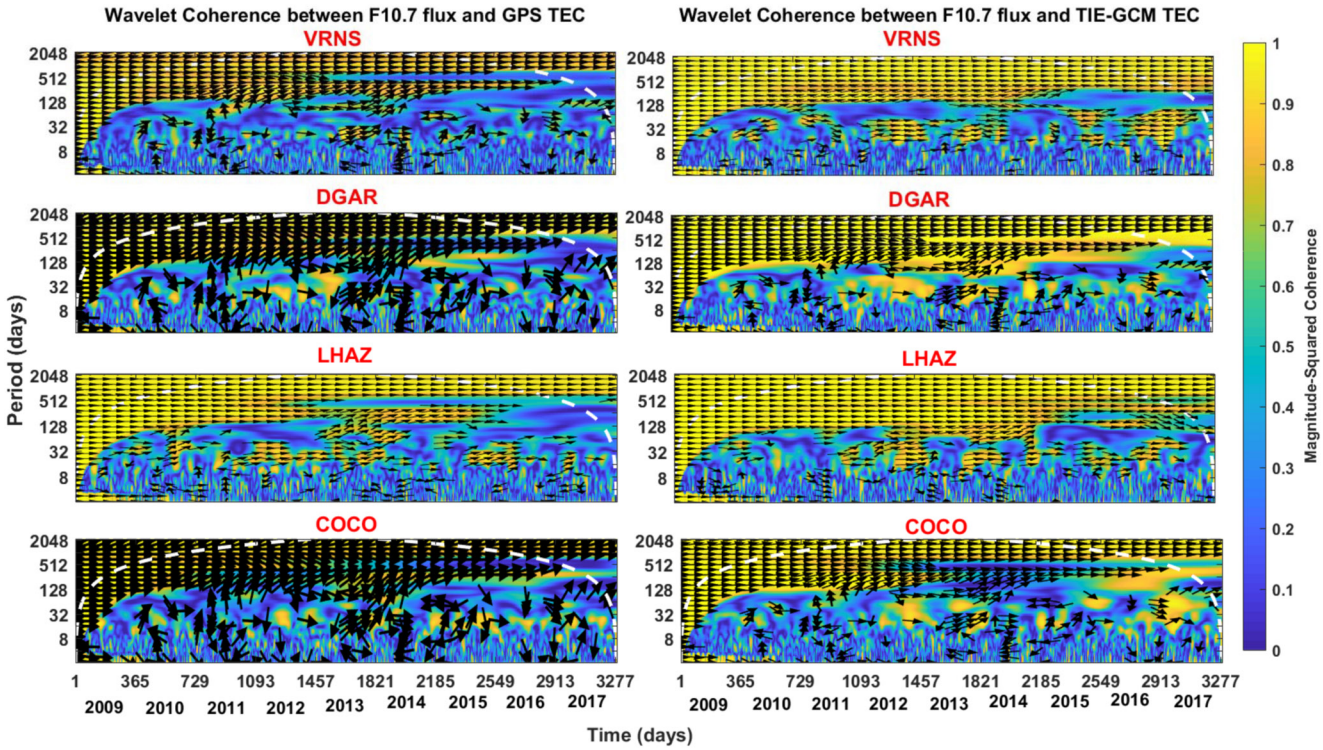

Figure 8. The wavelet coherence spectrum between F10.7 flux and Global Positioning System (GPS)-Total Electron Content (TEC) (left panel) time series and between F10.7 flux and Thermosphere-Ionosphere-Electrodynamics General Circulation Model (TIE-GCM) TEC (right panel) time series is presented.

the fountain effect in the EIA region as a potential candidate for the seeding of ionospheric QBO should not be disregarded (Chen, 1992; Lu et al., 2009). Sun et al. (2022) proposed that the QBO signals in the zonal wind in the mesosphere propagate upward into the E-region ionosphere and that QBO signals in the tidal winds in the E-region ionosphere modulate QBO signals in the EEJ through a global tidal wind-driven dynamo. Tang et al. (2014) calculated the QBO for the EIA region (150° geomagnetic latitude) using the TEC time series, which yields spectral peaks around 24 and 30 months corresponding to the stratospheric QBO. The strong or weak presence of particular components of QBO in TEC time series at land-locked/sea-locked stations may be closely related to atmospheric pressure loading (Pan et al., 2015). The quasi-biennial signal's mechanism, particularly with regard to lower atmospheric conditions, is yet unknown. Also, the latitudinal phase reversal of ~6–15 months lags at both sides of the equator in QBO of stratospheric zonal winds (Echer, 2007) may also be a possible factor for the appearance of a particular QBO period on any side of the equator. The stratospheric QBO are affected by the Ocean-Atmospheric coupling process (Jaiser et al., 2013). But there isn't enough evidence to explain the existence or absence of certain QBO in TEC and how they relate to lower atmospheric conditions, notably the oceanic environment.

To identify the relationships among TEC, solar, and geomagnetic indices in a time-frequency framework, we applied the wavelet coherence analysis to 365-day--smoothed-running-mean data. Here it is important to specify that the wavelet coherence analysis does not handle missing data points, and therefore we did not perform coherence analysis on the daily data of TEC. The wavelet coherence spectrum between the F10.7 flux & TEC and Ap & TEC time series are presented in Figures 8 and 9, respectively. The squared coherency is used to identify frequency bands within which two-time series are co-varying and is a measure of the intensity of the covariance of the two series in time-frequency space. The spurious wavelet periodicities are excluded by drawing the cone of influence (Torrence & Compo, 1998). Thus, we considered only those significant periodicities inside the cone of influence shown by white-shaded zones over the contour and a squared coherence magnitude greater than 0.5 (Figures 8 and 9). The phase display threshold is fixed at 0.5, which shows phase arrows only where the coherence is greater than or equal to 0.5. The arrows shown over the contour give the phase coherency between two time series. The phase relationship is determined in an anticlockwise direction, starting from 0° at the horizontal

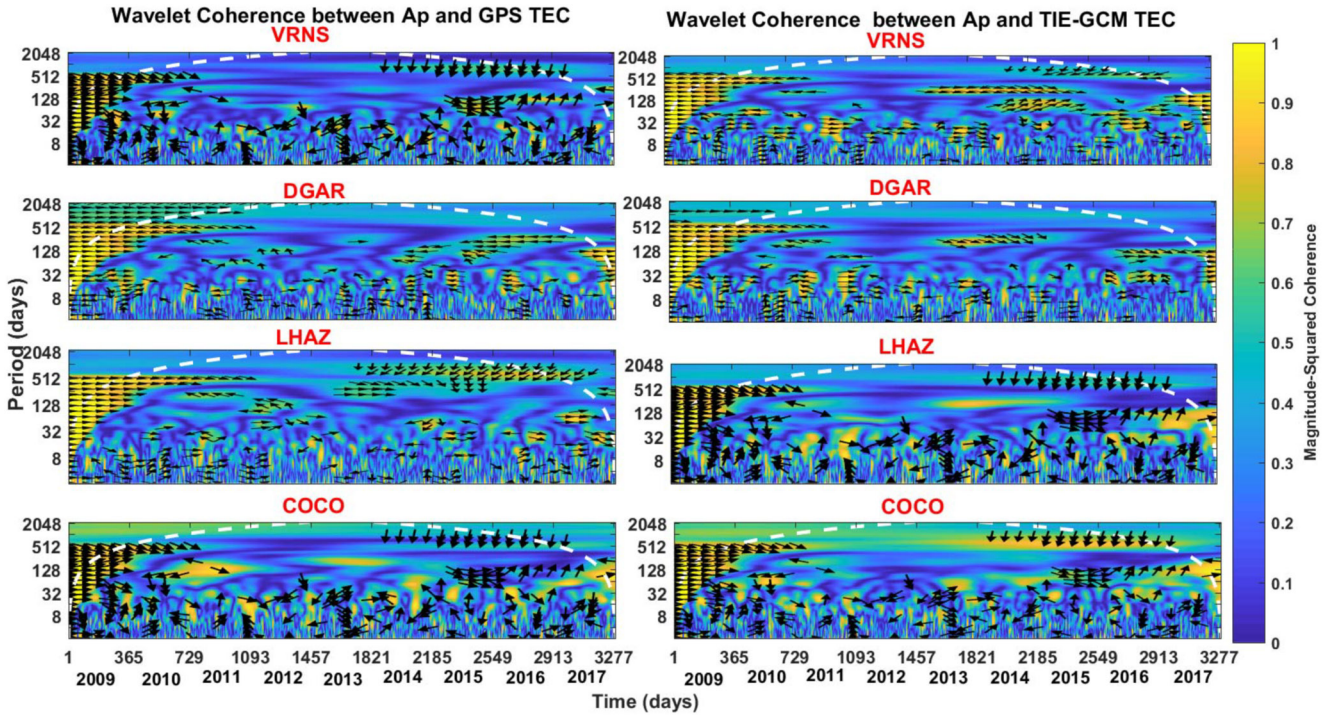

Figure 9. The wavelet coherence spectrum between Ap indices and Global Positioning System (GPS)-Total Electron Content (TEC) (left panel) time series and between Ap indices and Thermosphere-Ionosphere-Electrodynamics General Circulation Model (TIE-GCM) TEC (right panel) time series is presented.

right. The arrows represent the high coherency and linear relationship between two signals arrows at 0° (in phase) and 180° (anti of phase). The arrows at 90° (vertically up) and 270° (vertically down) indicate an out-of-phase and non-linear relationship between the two signals (e.g., Soon et al., 2014; Velasco Herrera et al., 2018).

It can be seen from Figure 8 that all existing QBO periodicities in TEC (GPS and TIE-GCM) greater than 550-day are highly coherent and in phase with F10.7 flux. The arrows corresponding to these periods align horizontally to the right; thus, both the time series are in phase. Consistent with the strong coherency noted from the coherence spectrum for QBO oscillations of the 730–775 -days (~2-year) period in TEC, the same period has been reported in almost all indices of solar activity (Apostolov, 1985; Soukharev & Hood, 2001; Zaqarashvili et al., 2010). However, a periodicity of 500-day in GPS TEC is not consistent with the F10.7 flux, particularly for 2012–2017. Contrary to this, a significant coherency and phase relationship is seen between the F10.7 flux and the TIE-GCM TEC time series for periodicities greater than the annual component. It can be seen from Figure 9 that no coherency exists for most QBO oscillations between Ap indices and TEC time series (GPS and TIE-GCM). A limited out-of-phase coherency is seen between QBO in TEC and Ap indices during the declining phase of solar activity. This reveals a non-linear relationship among implicit phenomena causing variability in Ap indices and TEC. Thus, the QBO oscillations of periods >550 days are highly correlated with solar activity. Also, the squared coherence magnitude is observed at ~0.1, which indicates that the 505 days periodicity that is significantly observed in GPS TEC at VRNS, DGAR, and COCO and dimly appears at LHAZ may not have its source in the QBO mechanism of solar activity. As a result, the less significant appearance of 505-day periodicity in GPS TEC at LHAZ and the strong presence of stations located within the EIA region in GPS TEC could be attributed to equatorial electrodynamics. The Himalayan station LHAZ is an off-crest location; therefore, 505 days has little spectral power. According to Tang et al. (2014), the relatively higher values of QBO-like signals are confined within $\pm 20^{o}$ at both sides of the equator based on the local time dependence characteristics of EIA strength. The latest results of Sun et al. (2022) also showed that the EIA characterizes the QBO in TEC; however, we do not have any supporting evidence, and therefore it is an open question that needs a separate study. A careful look at the coherence spectrum shown in Figures 8 and 9 also reveals inherent periods smaller than the annual oscillations. Also, the coherence spectrum shown in Figures 8 and 9 shows the episodic presence of periodicity associated with solar rotation and its harmonics in F10.7 flux and Ap indices and TEC (GPS and TIE-GCM). A

certain coherency and phase relationship also exist between the two-time series. Because the data employed were 365-day-running-averages and an accurate picture of annual and shorter periods could not be obtained, we do not analyze these periodicities and their coherency with the F10.7 flux/Ap time series.

Thus, it is likely from the coherence spectrum analysis that the 597-day, 730-day, 773-day and 930-day have a connection with the QBO of solar activity. Such mid-term periodicities in F10.7 flux are thought to be affine to the underlying intrinsic solar magnetism or solar dynamo operation (Egeland et al., 2015). The 597-day (∼1.7-year) have been reported in different quasi-continuous solar indices (e.g., Bazilevskaya et al., 2016; Li et al., 2010; Mendoza et al., 2006; Valdés-Galicia & Velasco, 2008).

5. Conclusions

The present study uses GPS and TIE-GCM time series of the period 2009–2017 from land- and sea-locked low-latitude stations to investigate solar cycle trends, short- and mid-term oscillations in TEC. The main findings are summarized below.

1. The F10.7 flux and TEC measurements of solar cycle-24 have revealed the presence of the well-known Gnevyshev gap and solar hysteresis. The seasons, local time, longitude and latitude all have an effect on the pattern of solar hysteresis. At sea-locked southern low-latitude stations, the second solar maximum is slightly delayed. Multiple modulations in the TEC solar cycle trend are visible at the northern EIA crest location. The values of the solar maxima are found to be greater at southern low-latitude stations than at northern low-latitude geomagnetic conjugate locations (Latitudinally). The values of solar maxima are higher along geomagnetic conjugate locations VRNS and DGAR than COCO and LHAZ (Longitudinally). In the case of GPS TEC, land-locked northern low-latitude stations exhibit clockwise hysteresis, whereas sea-locked stations exhibit mix-up hysteresis. TIE-GCM shows clockwise hysteresis at all stations.
2. The GPS TEC time series did not yield the periodicities of the solar rotation and its first harmonic (27-day and 13.5-day), but the TIE-GCM time series with sidebands of 28–30 -day did.
3. The TIE-GCM model has been shown to be capable of simulating semi-annual oscillations (182-day) as well as annual oscillations (365 ± 25 days). Inconsistency in the hemispheric asymmetry of semi-annual and annual components in the TIE-GCM time series, on the other hand, indicates that the model still needs appropriate modifications.
4. The 280-day inter-annual component has been observed in the F10.7 flux, and GPS TEC time series at northern landlocked low-latitude stations. At southern sea-locked low-latitude stations, it did not appear in the GPS TEC time series. This is an intriguing finding that suggests the presence of a seasonal component in TEC at northern low-latitudes but not at southern low-latitudes. In contrast, a 280-day periodicity appears in the TIE-GCM time series at both northern and southern low-latitude stations. Thus, the appearance of 280-day period in TIE-GCM TEC at southern low-latitude stations contradicts the GPS TEC observations and facts. That may be because the TIE-GCM does not account for solar flux, hemispheric and regionally dependent behaviour of the seasonal anomaly, and thus, the TIE-GCM presumes the seasonal component in TEC at southern low-latitude. The modifications made in the updated TIE-GCM version 2.0 by imposing seasonally variable eddy diffusion still need to solve the chemistry involved in seasonal variations.
5. The 120-day and 505-day periodicities have been observed significantly in GPS TEC at the northern EIA crest location of Varanasi and the southern EIA crest locations of DGAR and COCO Island, but did not appear at the northern off-crest location of LHAZ. It is intriguing to note that the 120- and 505-day periods do not appear in either the F10.7 flux or the Ap index, which the spectral coherence analysis has also verified. It follows that the 120- and 505-day intervals must be related to EIA electrodynamics. However, we do not have any supporting evidence; thus, this is an open research query to identify the cause of the absence of 505-day periods outside of the EIA region.
6. The F10.7 flux and TEC (GPS and TIE-GCM) time series at all stations had QBO periodicities of 587-, 730-, and 773-day. However, the spectral peak at 930-day is obtained in the F10.7 flux and GPS TEC time series only, and it did not appear in the TIE-GCM time series at any of the stations. The wavelet coherence analysis has also been used to identify the cause of the QBO oscillation in TEC, which reveals that the TEC QBO oscillations are highly coherent and in-phase with the QBO oscillation of the F10.7 flux. The wavelet coherence analysis revealed no clear correlation between TEC and QBO oscillations in geomagnetic activity. Nevertheless, in a few cases, some episodic and out-of-phase relationships exist. So, variations in solar activity are the primary source of ionospheric QBO oscillations.

Data Availability Statement

TEC data of chosen IGS stations in this analysis were obtained using file transfer protocol (ftp) access through the link: http://garner.ucsd.edu. Access to TEC data products requires user registration at Crustal Dynamics Data Information System (CDDIS) website https://cddis.nasa.gov/archive/gnss/data. A registered user can download IGS TEC data through html or ftp access. Alternatively, the IGS TEC used in the present analysis is available at the link; http://www.igs.gnsswhu.cn/index.php/home/data_product/igs.html, which does not require user registration. The monthly TEC data files of TIE-GCM runs were published in the "Runs on Request: IT Simulations Results" interface on the CCMC website link: https://ccmc.gsfc.nasa.gov. To access TIE-GCM data used in the present work, follow the following instructions at link- https://ccmc.gsfc.nasa.gov; click "Simulation Services" > click "View ROR Simulation Results" > select "Ionosphere/Thermosphere Model Results"> select "TIE-GCM"> click "View Runs." In the View Runs window user can find published TIE-GCM runs with run registration number sardar_rao_xxxxxx_IT_y. Here, *x* stands for the date of the model run, and *y* is the run number. The F10.7 flux data are accessible through the link: https://www.spaceweather.gc.ca/forecast-prevision/solar-solaire/solarflux/sx-5-en.php and the Ap index data is available at the World Wide Data center (https://wdc.kugi.kyoto-u.ac.jp/kp/index.html#LIST).

Acknowledgments
The Council of Scientific and Industrial Research (CSIR), New Delhi, funded this research through the Scientist's Pool Scheme awarded to Senior Research Associate Dr. Sardar Singh Rao (File No. 13 (9203-A)/2021- POOL dated 28/12/2021). The work of D. Chakrabarty is supported by the Department of Space, Government of India. The authors are thankful to the Community Coordinated Modeling Center, NASA, for TIE-GCM runs on request. Authors gratefully acknowledge Professor A. K. Singh, Department of Physics, Institute of Science, BHU Varanasi, India for allowing use of GPS TEC data of Varanasi. The authors thank both reviewers for meticulously evaluating the manuscript and giving valuable suggestions.

References

Adimula, I. A., Oladipo, O. A., & Adebiyi, S. J. (2016). Latitudinal and seasonal investigations of storm-time TEC variation. *Pure and Applied Geophysics*, *173*(7), 2521–2533. https://doi.org/10.1007/s00024-016-1291-2

Adler, N. O., & Elias, A. G., (2008). Latitudinal variation of foF2 hysteresis of solar cycles 20, 21, and 22. *Annales Geophysicae*, *26*, 1269–1273. https://doi.org/10.5194/angeo-26-1269-2008

Apostolov, E. M. (1985). Quasi-biennial oscillation in sunspot activity. *Astronomical Institutes of Czechoslovakia, Bulletin*, *36*(2), 97–102.

Appleton, E. V., & Piggott, W. R. (1955). *Physics of the ionosphere*. London: The Physical Society. 219–228.

Bai, T., & Sturrock, P. A. (1987). On the 152-day periodicity of the solar flare occurrence rate. *Nature*, *327*(6123), 601–604. https://doi.org/10.1038/327601a0

Bazilevskaya, G. A., Kalinin, M. S., Krainev, M. B., Makhmutov, V. S., Svirzhevskaya, A. K., Svirzhevsky, N. S., & Stozhkov, Y. I. (2016). On the relationship between quasi-biennial variations of solar activity, the heliospheric magnetic field and cosmic rays. *Cosmic Research*, *54*, 171–177. https://doi.org/10.1134/S0010952516010019

Berson, F. A., & Kulkarni, R. N. (1968). Sunspot cycle and the quasi-biennial oscillation. *Nature*, *217*, 1133–1134. https://doi.org/10.1038/2171133a0

Birch, M. J., Hargreaves, J. K., & Bailey, G. J. (2002). On the use of an effective ionospheric height in electron content measurement by GPS reception. *Radio Science*, *37*, 1–19. https://doi.org/10.1029/2000rs002601

Cameron, R. H., Dasi-Espuig, M., Jiang, J., Işık, E., Schmitt, D., & Schüssler, M. (2013). Limits to solar cycle predictability: Cross-equatorial flux plumes. *Astronomy and Astrophysics*, *557*(A141), 6. https://doi.org/10.1051/0004-6361/201321981

Chakrabarty, D., Bagiya, M. S., Thampi, S. V., & Iyer, K. N. (2012). Solar EUV flux (0.1-50 nm), F10.7 cm flux, sunspot number and the total electron content in the crest region of equatorial ionization anomaly during the deep minimum between solar cycle 23 and 24. *Indian Journal of Radio and Space Physics*, *41*(2), 110–120.

Chakraborty, S. K., & Hajra, R. (2007). Solar control of ambient ionization of the ionosphere near the crest of the equatorial anomaly in the Indian zone. *Bulletin of Astrophysics Society of India*, *35*, 599–605.

Chakraborty, S. K., & Hajra, R. (2008). Solar control of ambient ionization of the ionosphere near the crest of the equatorial anomaly in the Indian zone. *Annals of Geophysics*, *26*, 47–57. https://doi.org/10.5194/angeo-26-47-2008

Chandrasekhar, E., Sanjana, S. P., Seemala, G. K., & Shenvi, N. (2016). Multifractal detrended fluctuation analysis of ionospheric total electron content data during solar minimum and maximum. *Journal of Atmospheric and Solar-Terrestrial Physics*, *149*, 31–39. https://doi.org/10.1016/j.jastp.2016.09.007

Chanin, M. L., Keckhut, P., Hauchecorne, A., & Labitzke, K. (1989). The solar activity-QBO effect in the lower thermosphere. *Annales Geophysicae*, *32*, 225–230.

Chen, P.-R. (1992). Evidence of the ionospheric response to the QBO. *Geophysical Research Letters*, *19*, 1089–1092. https://doi.org/10.1029/91GL01564

Codrescu, M. V., Palo, S. E., Zhang, X., Fuller-Rowell, T. J., & Poppe, C. (1999). TEC climatology derived from TOPEX/POSEIDON measurements. *Journal of Atmospheric and Solar-Terrestrial Physics*, *61*(3–4), 281–298. https://doi.org/10.1016/S1364-6826(98)00132-1

Danilov, A. D., & Mikhailov, A. V. (1999). Spatial and seasonal variations of the foF2 long-term trends. *Annales Geophysicae*, *17*, 1239–1243. https://doi.org/10.1007/s00585-999-1239-2

De Abreu, A. J., Martin, I. M., De Jesus, R., Bolzan, M. J. A., Venkatesh, K., Fagundes, P. R., et al. (2017). Comparison of GPS-TEC measurements with IRI2012-TEC predictions in the Brazilian sector during the unusual solar minimum 2009. *Annales Geophysicae*, *60*, 0331. https://doi.org/10.4401/ag-7300

de Gonzalez, A. L. C., Gonzalez, W. D., Dutra, S. L. G., & Tsurutani, B. T. (1993). Periodic variation in the geomagnetic activity: A study based on the Ap index. *Journal of Geophysical Research*, *98*(A6), 9215–9231. https://doi.org/10.1029/92ja02200

Donelly, R. F., & Puga, L. C. (1990). 13 day periodicity and the center to limb dependence of UV, EUV and X-ray emission of solar activity. *Solar Physics*, *130*, 369–390. https://doi.org/10.1007/BF00156800

Dunkerton, T. J. (1997). The role of gravity waves in the quasi-biennial oscillation. *Journal of Geophysical Research*, *102*, 26053–26076. https://doi.org/10.1029/96JD02999

Echer, E. (2007). On the quasi-biennial oscillation (QBO) signal in the foF2 ionospheric parameter. *Journal of Atmospheric and Solar-Terrestrial Physics*, *69*(4–5), 621–627. https://doi.org/10.1016/j.jastp.2006.11.001

Egeland, R., Metcalfe, T., Hall, J. C., & Henry, G. W. (2015). SUN-like magnetic cycles in the rapidly rotating young solar analog hd 30495. *The Astrophysical Journal*, *812*(12), 11. https://doi.org/10.1088/0004-637X/812/1/12

Elias, A. G. (2014). Filtering ionosphere parameters to detect trends linked to anthropogenic effects. *Earth Planets and Space*, *66*, 113. https://doi.org/10.1186/1880-5981-66-113

Emery, B. A., Coumans, V., Evans, D. S., Germany, G. A., Greer, M. S., Holeman, E., et al. (2008). Seasonal, Kp, solar wind, and solar flux variations in long-term single-pass satellite estimates of electron and ion auroral hemispheric power. *Journal of Geophysical Research*, *113*, A06311. https://doi.org/10.1029/2007JA012866

Fejer, B. G., Gonzales, C. A., Farley, D. T., Kelley, M. C., & Woodman, R. F. (1979). Equatorial electric fields during magnetically disturbed conditions: 1. The effect of the interplanetary magnetic field. *Journal of Geophysical Research*, *84*(A10), 5797–5802. https://doi.org/10.1029/JA084iA10p05797

Forbes, J. M. (1996). Planetary waves in the thermosphere-ionosphere system. *Journal of Geomagnetism and Geoelectricity*, *48*(1), 91–98. https://doi.org/10.5636/jgg.48.91

Forbes, J. M., Maute, A., Zhang, X., & Hagan, M. E. (2018). Oscillation of the ionosphere at planetary-wave periods. *Journal of Geophysical Research: Space Physics*, *123*, 7634–7649. https://doi.org/10.1029/2018JA025720

Forbes, J. M., Palo, S. E., & Zhang, X. (2000). Variability of the ionosphere. *Journal of Atmospheric and Solar-Terrestrial Physics*, *62*(8), 685–693. https://doi.org/10.1016/S1364-6826(00)00029-8

Fuller-Rowell, T. J. (1998). The "thermospheric spoon": A mechanism for the semiannual density variation. *Journal of Geophysical Research*, *103*, 3951–3956. https://doi.org/10.1029/97JA03335

Garcia, R. R., & Solomon, S. (1985). The effect of breaking gravity waves on the dynamics and chemical composition of the mesosphere and lower thermosphere. *Journal of Geophysical Research*, *90* (D2), 3850–3868. https://doi.org/10.1029/JD090iD02p03850

Gnevyshev, M. N. (1963). The corona and the 11-year cycle of solar activity. *Soviet Astronomy*, *7*, 311.

Gnevyshev, M. N. (1967). On the 11-years cycle of solar activity. *Solar Physics*, *1*, 107–120. https://doi.org/10.1007/BF00150306

Goncharenko, L. P., Chau, J. L., Liu, H.-L., & Coster, A. J. (2010). Unexpected connections between the stratosphere and ionosphere. *Geophysical Research Letters*, *37*, 10101. https://doi.org/10.1029/2010gl043125

Guo, J., Li, W., Liu, X., Kong, Q., Zhao, C., & Guo, B. (2015). Temporal-spatial variation of global GPS-derived total electron content, 1999-2013. *PLoS One*, *10*(7), e0133378. https://doi.org/10.1371/journal.pone.0133378

Hagan, M. E., & Forbes, J. M. (2002). Migrating and nonmigrating diurnal tides in the middle and upper atmosphere excited by tropospheric latent heat release. *Journal of Geophysical Research*, *107*(D24), 4754. https://doi.org/10.1029/2001JD001236

Hajra, R., Chakraborty, S. K., Tsurutani, B. T., DasGupta, A., Echer, E., Brum, C. G. M., et al. (2016). An empirical model of ionospheric total electron content (TEC) near the crest of the equatorial ionization anomaly (EIA). *Journal of Space Weather and Space Climate*, *6*, 1–9. https://doi.org/10.1051/swsc/2016023

Hargreaves, J. K. (1992). *The solar–terrestrial environment*. Cambridge: Cambridge University Press. https://doi.org/10.1017/CBO9780511628924

Heelis, R. A., Lowell, J. K., & Spiro, R. W. (1982). A model of the high-latitude convection pattern. *Journal of Geophysical Research*, *87*, 6339–6345. https://doi.org/10.1029/ja087ia08p06339

Holton, J. R., & Lindzen, R. S. (1972). An updated theory for the quasi-biennial cycle of the tropical stratosphere. *29*(6), 1076–1080. *Journal of the Atmospheric Sciences*, https://doi.org/10.1175/1520-0469(1972)029<1076:autftq>2.0.co;2

Horne, J. H., & Baliunas, S. L. (1986). A prescription for period analysis of unevenly sampled time series. *Astrophysics Journal*, *302*, 757–763. https://doi.org/10.1086/164037

Huang, Y.-N., & Jeng, B. S. (1976). A further study on the hysteresis variation of the F2-layer semi-thickness parameter ypF2 at Kokubunji, Japan. *Journal of Atmospheric and Terrestrial Physics*, *38*(3), 319–323. https://doi.org/10.1016/0021-9169(76)90101-X

Huo, X. L., Yuan, Y. B., Ou, J. K., Zhang, K. F., & Bailey, G. J. (2009). Monitoring the global-scale winter anomaly of total electron contents using GPS data. *Earth Planets and Space*, *61*, 1019–1024. https://doi.org/10.1186/BF03352952

Ikubanni, S. O., Adeniyi, J. O., Adebesin, B. O., & Adebiyi, S. J. (2019). Dynamics of sunspot cycle ascending and descending phases asymmetry in equatorial ionospheric variability. *Journal of Atmospheric and Solar-Terrestrial Physics*, *182*, 25–30. https://doi.org/10.1016/j.jastp.2018.10.017

Immel, T. J., Sagawa, E., England, S. L., Henderson, S. B., Hagan, M. E., Mende, S. B., et al. (2006). Control of equatorial ionospheric morphology by atmospheric tides. *Geophysical Research Letters*, *33*(15), L15108. https://doi.org/10.1029/2006GL026161

Jaiser, R., Dethloff, K., & Handorf, D. (2013). Stratospheric response to Arctic sea ice retreat and associated planetary wave propagation changes. *Tellus A: Dynamic Meteorology and Oceanography*, *65*(1), 1–11. https://doi.org/10.3402/tellusa.v65i0.19375

Jee, G., Schunk, R. W., & Scherliess, L. (2004). Analysis of TEC data from the TOPEX/Poseidon mission. *Journal of Geophysical Research*, *109*(A1), A01301. https://doi.org/10.1029/2003ja010058

Jethva, C., Bagiya, M. S., & Joshi, H. P. (2022). On the GPS TEC variability for full solar cycle and its comparison with IRI-2016 model. *Astrophysics and Space Science*, *367*, 80. https://doi.org/10.1007/s10509-022-04112-y

Kalita, B. R., Bhuyan, P. K., Nath, S. J., Choudhury, M. C., Chakrabarty, D., Wang, K., et al. (2022). The investigation on daytime conjugate hemispheric asymmetry along 100°E longitude using observations and model simulations: New insights. *Advances in Space Research*, *69*(10), 3726–3740. https://doi.org/10.1016/j.asr.2022.02.058

Kane, R. P. (1995). Quasi-biennial oscillation in ionospheric parameters measured at Juliusruch (55N, 13E). *Journal of Atmospheric and Solar-Terrestrial Physics*, *57*, 415–419. https://doi.org/10.1016/0021-9169(95)90046-s

Kane, R. P. (2002). Periodicities in the time series of solar coronal radio emissions and chromospheric UV emission lines. *Solar Physics*, *205*, 351–359. https://doi.org/10.1023/A:1014253824687

Kane, R. P. (2003). Fluctuations in the ∼27-day sequences in the solar index F10 during solar cycles 22–23. *Journal of Atmospheric and Solar-Terrestrial Physics*, *65*(10), 1169–1174. https://doi.org/10.1016/S1364-6826(03)00167-6

Kane, R. P. (2005). Differences in the quasi-biennial oscillation and quasi-triennial oscillation characteristics of the solar, interplanetary and terrestrial parameters. *Journal of Geophysical Research*, *110*(A1), A01108. https://doi.org/10.1029/2004JA010606

Kane, R. P. (2009). Early history of cosmic rays and solar wind-some personal remembrances. *Advances in Space Research*, *44*, 1252–1255. https://doi.org/10.1016/j.asr.2008.10.041

Kane, R. P. (2010). Gnevyshev peaks in the CME average speeds in cycle 23. *Solar Physics*, *261*, 209–213. https://doi.org/10.1007/s11207-009-9466-y

Karak, B. B., Mandal, S., & Banerjee, D. (2018). Double peaks of the solar cycle: An explanation from a dynamo model. *The Astrophysical Journal*, *866*, 17. https://doi.org/10.3847/1538-4357/aada0d

Khattatov, B. V., Geller, M. A., Yubin, V. A., Yubin, V. A., & Hays, P. B. (1997). Diurnal migrating tides as seen by the high-resolution doppler imager/UARS 2. Monthly mean global zonal and vertical velocities, pressure, temperature, and inferred dissipation. *Journal of Geophysical Research*, *102*(D4), 4423–4435. https://doi.org/10.1029/96JD03654

Kitchatinov, L. L., Mordvinov, A. V., & Nepomnyashchikh, A. A. (2018). Modelling variability of solar activity cycles. *Astronomy and Astrophysics*, *615*, 1–8. https://doi.org/10.1051/0004-6361/201732549

Krainev, M. B., Bazilevskaya, G. A., & Sladkova, A. I. (1997). The cosmic ray intensity in the periods of the inversion of high latitude solar magnetic field. In *Modem problems of solar cycle Pulkovo*, 362–366.

Kurt, K., Yeşil, A., Sağir, S., & Atici, R. (2016). The relationship of stratospheric QBO with the difference of measured and calculated NmF2. *Acta Geophysica*, *64*(6), 2781–2793. https://doi.org/10.1515/acgeo-2016-0061

Lean, J. L., Meier, R. R., Picone, J. M., & Emmert, J. T. (2011). Ionospheric total electron content: Global and hemispheric climatology. *Journal of Geophysical Research: Space Physics*, *116*, A10318. https://doi.org/10.1029/2011JA016567

Lean, J. L., Meier, R. R., Picone, J. M., Sassi, F., Emmert, J. T., & Richards, P. G. (2016). Ionospheric total electron content: Spatial patterns of variability. *Journal of Geophysical Research: Space Physics*, *121*, 10367–10402. https://doi.org/10.1002/2016ja023210

Lee, W. K., Kil, H., Kwak, Y. S., Wu, Q., Cho, S., & Park, J. U. (2011). The winter anomaly in the middle-latitude F region during the solar minimum period observed by the constellation observing system for meteorology, ionosphere, and climate. *Journal of Geophysical Research: Space Physics*, *116*, A02302. https://doi.org/10.1029/2010JA015815

Li, K. J., Xu, J. C., Liu, X. H., Gao, P. X., & Zhan, L. S. (2010). Periodicity of total solar irradiance. *Solar Physics*, *267*, 295–303. https://doi.org/10.1007/s11207-010-9655-8

Li, S., Peng, J., Xu, W., & Qin, K. (2013). Time series modeling and analysis of trends of daily averaged ionospheric total electron content. *Advances in Space Research*, *52*, 801–809. https://doi.org/10.1016/j.asr.2013.05.032

Lin, C. H., Richmond, A. D., Heelis, R. A., Bailey, G. J., Lu, G., Liu, J. Y., et al. (2005). Theoretical study of the low- and mid-latitude ionospheric electron density enhancement during the October 2003 superstorm: Relative importance of the neutral wind and the electric field. *Journal of Geophysical Research*, *110*, A12312. https://doi.org/10.1029/2005JA011304

Liu, H., Stolle, C., Forster, M., & Watanabe, S. (2007). Solar activity dependence of the electron density in the equatorial anomaly regions observed by CHAMP. *Journal of Geophysical Research: Space Physics*, *112*, 311. https://doi.org/10.1029/2007ja012616

Lockwood, M., McWilliams, K. A. M., Owens, M. J., Barnard, L. A., Watt, C. E., Scott, C. J., et al. (2020). Semi-annual, annual and universal time variations in the magnetosphere and in geomagnetic activity: 2. Response to solar wind power input and relationships with solar wind dynamic pressure and magnetospheric flux transport. *Journal of Space Weather Space Climate*, *10*, 1–24. https://doi.org/10.1051/swsc/2020033

Lu, H., Gray, L. J., Baldwin, M. P., & Jarvis, M. J. (2009). Life cycle of the QBO-modulated 11-year solar cycle signals in the Northern Hemispheric winter. *Quarterly Journal of the Royal Metrological Society*, *135* (641), 1030–1043. https://doi.org/10.1002/qj.419

Ma, L. H., Han, Y. B., & Yin, Z. Q. (2009). Periodicities in global mean TEC from GNSS observations. *Earth, Moon, and Planets*, *105*, 3–10. https://doi.org/10.1007/s11038-008-9242-2

Maliniemi, V., Asikainen, T., & Mursula, K. (2016). Effect of geomagnetic activity on the northern annular mode: QBO dependence and the holton-tan relationship. *Journal of Geophysical Research: Atmosphere*, *121*, 10043–10055. https://doi.org/10.1002/2015JD024460

Mannucci, A. J., Wilson, B. D., & Edwards, C. D. (1993). *A new method for monitoring the Earth's ionospheric total electron content using the GPS global network*. Paper presented at ION GPS-93, Institute of Navigation. 1323–1332. Retrieved%20from%20http://hdl.handle.net/2014/36277

Mansilla, G. A., Mosert, M., & Ezquer, R. (2005). Seasonal variation of the total electron content, maximum electron density and equivalent slab thickness at a South-American station. *Journal of Atmospheric and Solar-Terrestrial Physics*, *67*, 1687–1690. https://doi.org/10.1016/j.jastp.2005.02.024

Maute, A. (2017). Thermosphere-ionosphere-electrodynamics general circulation model for the ionospheric connection explorer: TIEGCM-ICON. *Space Science Reviews*, *212*(1–2), 523–551. https://doi.org/10.1007/s11214-017-0330-3

McIntosh, S., Leamon, R., Krista, L. D., Title, A. M., Hudson, H. S., Riley, P., et al. (2015). The solar magnetic activity band interaction and instabilities that shape quasi-periodic variability. *Nature Communications*, *6*, 6491. https://doi.org/10.1038/ncomms7491

Mendillo, M., Huang, C. L., Pi, X., Rishbeth, H., & Meier, R. (2005). The global ionospheric asymmetry in total electron content. *Journal of Atmospheric and Solar-Terrestrial Physics*, *67*(15), 1377–1387. https://doi.org/10.1016/j.jastp.2005.06.021

Mendoza, B., Velasco, V. M., & Valdés-Galicia, J. F. (2006). Mid-term periodicities in the solar magnetic flux. *Solar Physics*, *233*, 319–330. https://doi.org/10.1007/s11207-006-4122-2

Mikhailov, A. V., & Mikhailov, V. V. (1995). Solar cycle variations of annual mean noon foF2. *Advances in Space Research*, *15*(2), 79–82. https://doi.org/10.1016/s0273-1177(99)80026-x

Mikhailov, A. V., & Perrone, L. (2014). Comment on ''The winter anomaly in the middle-latitude F region during the solar minimum period observed by the constellation Observing System for Meteorology, Ionosphere, and Climate'' by W. K. Lee, H. Kil, Y.-S. Kwak, Q. Wu, S. Cho, and J. U. Park. *Journal of Geophysical Research: Space Physics*, *119*, 7972–7978. https://doi.org/10.1002/2014JA020185

Mursula, K., & Zieger, B. (1996). The 13.5 day periodicity in the sun, solar wind and geomagnetic activity. *Journal of Geophysical Research*, *101*(A12), 27077–27090. https://doi.org/10.1029/96JA02470

Nayar, S. R. P., Alexander, L. T., Radhika, V. N., John, T., Subrahmanyam, P., Chopra, P., et al. (2004). Observation of periodic fluctuations in electron and ion temperatures at the low-latitude upper ionosphere by SROSS-C2 satellite. *Annales Geophysicae*, *22*(5), 1665–1674. Retrieved from https://hal.archives-ouvertes.fr/hal-00317346

Nayar, S. R. P., Nair, V. S., Radhika, V. N., & Revathy, K. (2001). Short period features of the interplanetary plasma and their evolution. *Solar Physics*, *201*(2), 405–417. https://doi.org/10.1023/A:1017599621110

Nayar, S. R. P., Nair, V. S., Radhika, V. N., Revathy, K., & Ramadas, V. (2002). Wavelet analysis of periodicities in interplanetary medium. *Solar Physics*, *212*, 207–211.

Neumann, A. (1990). QBO and solar activity effects on temperatures in the mesopause region. *Journal of Atmospheric and Solar-Terrestrial Physics*, *52*(3), 165–173. https://doi.org/10.1016/0021-9169(90)90120-C

Norton, A. A., & Gallagher, J. C. (2010). Solar-cycle characteristics examined in separate hemispheres: Phase, Gnevyshev gap, and length of minimum. *Solar Physics*, *261*, 193–207. https://doi.org/10.1007/s11207-009-9479-6

Ouattara, F., & Amory-Mazaudier, C. (2012). Statistical study of the equatorial F2 layer at Ouagadougou during solar cycles 20, 21 and 22, using legrand and simon's classification of geomagnetic activity. *Journal of Space Weather and Space Climate*, *2*, A19. https://doi.org/10.1051/swsc/2012019

Ozguc, A., Atac, T., & Pektas, R. (2008). Examination of the solar cycle variation of foF2 for cycles 22 and 23. *Journal of Atmospheric and Solar-Terrestrial Physics*, *70*, 268–276. https://doi.org/10.1016/j.jastp.2007.08.016

Pan, Y., Shen, W. B., Ding, H., Hwang, C., Li, J., Zhang, T., et al. (2015). The quasi-biennial vertical oscillations at global GPS stations: Identification by ensemble empirical mode decomposition. *Sensors*, *15*(10), 26096–26114. https://doi.org/10.3390/s151026096

Pilinski, M. D., & Crowley, G. (2015). Seasonal variability in global eddy diffusion and the effect on neutral density. *Journal of Geophysical Research: Space Physics*, *120*, 3097–3117. https://doi.org/10.1002/2015JA021084

Qian, L., Burns, A. G., Solomon, S. C., & Wang, W. (2013). Annual/semiannual variation of the ionosphere. *Geophysical Research Letters*, *40*, 1928–1933. https://doi.org/10.1002/grl.50448

Qian, L., & Solomon, S. C. (2012). Thermospheric density: An overview of temporal and spatial variations. *Space Science Reviews*, *168*, 147–173. https://doi.org/10.1007/s11214-011-9810-z

Qian, L., Solomon, S. C., & Kane, T. J. (2009). Seasonal variation of thermospheric density and composition. *Journal of Geophysical Research*, *114*, A01312. https://doi.org/10.1029/2008ja013643

Raja Rao, K. S., & Joseph, K. T. (1971). Quasi-biennial oscillation in the geomagnetic Sq field in the low latitude region. *Journal of Atmospheric and Terrestrial Physics*, *33*(5), 797–805. https://doi.org/10.1016/0021-9169(71)90032-8

Rao, M. S. V. G., & Rao, R. S. (1969). The hysteresis variation in F2-layer parameters. *Journal of Atmospheric and Solar-Terrestrial Physics*, *13*, 1119–1125. https://doi.org/10.1016/0021-9169(69)90110-X

Rao, S. S., Chakraborty, M., Sanjay, K., & Singh, A. K. (2019). Low latitude ionospheric response from GPS, IRI, and TIE-GCM TEC to solar cycle 24. *Astrophysics and Space Science*, *364*, 216. https://doi.org/10.1007/s10509-019-3701-2

Rao, S. S., Galav, P., Sharma, S., & Pandey, R. (2013). Low-latitude TEC variability studied from magnetically conjugate locations along 73°E longitude. *Journal of Atmospheric and Solar-Terrestrial Physics*, *104*, 1–6. https://doi.org/10.1016/j.jastp.2013.08.007

Rao, S. S., Sharma, S., & Pandey, R. (2019). Study of solar flux dependency of the winter anomaly in GPS TEC. *GPS Solutions*, *23*, 4. https://doi.org/10.1007/s10291-018-0795-x

Richards, P. G., Fennelly, J. A., & Torr, D. G. (1994). Euvac: A solar EUV flux model for aeronomic calculations. *Journal of Geophysical Research*, *99*(A5), 8981–8992. https://doi.org/10.1029/94JA00518

Richmond, A. D. (1992). Assimilative mapping of ionospheric electrodynamics. *Advances in Space Research*, *12*(6), 59–68. https://doi.org/10.1016/0273-1177(92)90040-5

Rishbeth, H. (1998). How the thermospheric circulation affects the ionospheric F_2-layer. *Journal of Atmospheric and Solar-Terrestrial Physics*, *60*(14), 1385–1402. https://doi.org/10.1016/S1364-6826(98)00062-5

Rishbeth, H. (2006). F-region links with the lower atmosphere? *Journal of Atmospheric and Solar-Terrestrial Physics*, *68*(3–5), 469–478. https://doi.org/10.1016/j.jastp.2005.03.017

Rishbeth, H., Ganguly, S., & Walker, J. C. G. (1978). Field-aligned and field-perpendicular velocities in the ionospheric F2-layer. *Journal of Atmospheric and Terrestrial Physics*, *40*(7), 767–784. https://doi.org/10.1016/0021-9169(78)90028-4

Rishbeth, H., & Mendillo, M. (2001). Patterns of F2-layer variability. *Journal of Atmospheric and Terrestrial Physics*, *63*(15), 1661–1680. https://doi.org/10.1016/S1364-6826(01)00036-0

Roble, R. G., Ridley, E. C., Richmond, A. D., & Dickinson, R. E. (1988). A coupled thermosphere/ionosphere general circulation model. *Geophysical Research Letters*, *15*(2), 1325–1328. https://doi.org/10.1029/GL015i012p01325

Russel, C. T., & McPherron, R. L. (1973). Semi-annual variation of geomagnetic activity. *Journal of Geophysical Research*, *78*(1), 92–108. https://doi.org/10.1029/JA078i001p00092

Russell, C. T. (1971). *Geophysical coordinate transformations*. Cambridge University Press, chapter. Appendix 3. 184–196. https://doi.org/10.1017/9781139878296.019

Scargle, J. D., (1982). Studies in astronomical time series analysis. II. Statistical aspects of spectral analysis of unevenly spaced data. *The Astrophysical Journal*, *263*, 835–853. https://doi.org/10.1086/160554

Schunk, R., & Nagy, A. (2009). *Ionospheres*. 2nd ed. Cambridge University Press, 260–264. https://doi.org/10.1017/CBO9780511635342

Schunk, R. W., & Nagy, A. F. (1978). Electron temperatures in the F region of the ionosphere: Theory and observations. *Reviews of Geophysics*, *16*(3), 355–399. https://doi.org/10.1029/RG016i003p00355

Seemala, G. K., & Valladares, C. E. (2011). Statistics of total electron content depletions observed over the South American continent for the year 2008. *Radio Science*, *46*, RS5019. https://doi.org/10.1029/2011RS004722

Shim, J.-S. (2009). Analysis of total electron content (TEC) variations in the low- and middle-latitude ionosphere. All Graduate Thesis and Dissertations. *403*. Retrieved%20from%20https://digitalcommons.usu.edu/etd/403

Solomon, S., Burns, A., Emery, B., Foster, B., Liu, H., Lu, G., et al. (2016). *Thermosphere-ionosphere-electrodynamics general circulation model (TIE-GCM)*. CEDAR Summer Workshop Santa Fe.

Soon, W., Velasco Herrera, V. M., Selvaraj, K., Traversi, R., Usoskin, I., Chen, C. T. A., et al. (2014). A review of Holocene solar-linked climatic variation on centennial to millennial timescales: Physical processes, interpretative frameworks and a new multiple cross-wavelet transform algorithm. *Earth-Science Reviews*, *134*, 1–15. https://doi.org/10.1016/j.earscirev.2014.03.003

Soukharev, B. E., & Hood, L. L. (2001). Possible solar modulation of the equatorial quasibiennial oscillation: Additional statistical evidence. *Journal of Geophysical Research*, *106*(D14), 14855–14868. https://doi.org/10.1029/2001JD900095

Storini, M. (1997). Cosmic rays for solar-terrestrial physics, II nuovo cimento, *2OC*, 871–880.

Su, Y. Z., Bailey, G. J., & Oyama, K.-I. (1998). Annual and seasonal variations in the low-latitude topside ionosphere. *Annals of Geophysics*, *16*, 974–985. https://doi.org/10.1007/s00585-998-0974-0

Sun, R., Gu, S.-Y., Dou, X., Zhang, R., Kuai, J., & Tsuda, T. (2022). The impact of the quasi-biennial oscillation on the mesosphere and ionosphere. *Journal of Geophysical Research: Space Physics*, *127*, e2021JA029920. https://doi.org/10.1029/2021ja029920

Sunda, S., & Vyas, B. M. (2013). Local time, seasonal, and solar cycle dependency of longitudinal variations of TEC along the crest of EIA over India. *Journal of Geophysical Research: Space Physics*, *118*, 6777–6785. https://doi.org/10.1002/2013ja018918

Tang, W., Xue, X.-H., Lei, J., & Dou, X.-K. (2014). Ionospheric quasi-biennial oscillation in global TEC observations. *Journal of Atmospheric and Solar-Terrestrial Physics*, *107*, 36–41. https://doi.org/10.1016/j.jastp.2013.11.002

Titheridge, J. E., & Buonsanto, M. J. (1983). Annual variations in the electron content and height of the F layer in the northern and southern hemispheres, related to neutral compositions. *Journal of Atmospheric and Solar-Terrestrial Physics*, *45*(10), 683–696. https://doi.org/10.1016/S0021-9169(83)80027-0

Torr, M. R., & Torr, D. G. (1973). The seasonal behaviour of the F2-layer of the ionosphere. *Journal of Atmospheric and Solar-Terrestrial Physics*, *35*, 2237–2251. https://doi.org/10.1016/0021-9169(73)90140-2

Torrence, C., & Compo, G. P. (1998). A practical guide to wavelet analysis. *Bulletin of the American Meteorological Society*, *79*, 61–78. https://doi.org/10.1175/1520-0477(1998)079<0061:apgtwa>2.0.co;2

Tsai, H., Liu, J., Tsai, W., Liu, C., Tseng, C.-L., & Wu, C.-C. (2001). Seasonal variations of the ionospheric total electron content in Asia equatorial anomaly regions. *Journal of Geophysical Research*, *106*(A12), 30363–30369. https://doi.org/10.1029/2001JA001107

Valdés-Galicia, J. F., & Velasco, V. M. (2008). Variations of mid-term periodicities in solar activity physical phenomena. *Advances in Space Research*, *41*(2), 297–305. https://doi.org/10.1016/j.asr.2007.02.012

Velasco Herrera, V. M., Pérez-Peraza, J., Soon, J. C., & Márquez-Adame, W. (2018). The quasi-biennial oscillation of 1.7 years in ground level enhancement events. *New Astronomy*, *60*, 7–13. https://doi.org/10.1016/j.newast.2017.09.007

Volland, H. (1995). *Handbook of atmospheric electrodynamics, volume I*. CRC Press, 432. https://doi.org/10.1201/9780203719503

Weimer, D. R. (2001). An improved model of ionospheric electric potentials including substorm perturbations and application to the geospace environment modeling november 24, 1996, event. *Journal of Geophysical Research*, *106*, 407–416. https://doi.org/10.1029/2000ja000604

Yasyukevich, Y. V., Yasyukevich, A. S., Ratovsky, K. G., Klimenko, M. V., Klimenko, V. V., & Chirik, N. V. (2018). Winter anomaly in NmF2 and TEC: When and where it can occur. *Journal of Space Weather and Space Climate*, *8*. https://doi.org/10.1051/swsc/2018036

Zaqarashvili, T. V., Carbonell, M., Oliver, R., & Ballester, J. L. (2010). Quasi-biennial oscillations in the solar tachocline caused by magnetic Rossby wave instabilities. *The Astrophysical Research Letters*, *724*, L95–L98. https://doi.org/10.1088/2041-8205/724/1/L95

Zhao, B., Wan, W., & Liu, L. (2005). Responses of equatorial anomaly to the October–November 2003 super storms. *Annals of Geophysics*, *23*(3), 693–706. https://doi.org/10.5194/angeo-23-693-2005

Zhao, B., Wan, W., Liu, L., Mao, T., Ren, Z., Wang, M., & Christensen, A. B. (2007). Features of annual and semiannual variations derived from the global ionospheric maps of total electron content. *Annals of Geophysics*, *25*, 2513–2527. https://doi.org/10.5194/angeo-25-2513-2007

Zhao, B., Wan, W., Liu, L., & Ren, Z. (2009). Characteristics of the ionospheric total electron content of the equatorial ionization anomaly in the Asian-Australian region during 1996-2004. *Annales Geophysicae*, *27*, 3861–3873. https://doi.org/10.5194/angeo-27-3861-2009

Zięba, S., Masłowski, J., Michalec, A., & Kułak, A. (2001). Periodicities in data observed during the minimum and the rising phase of solar cycle 23; years 1996–1999. *Astronomy and Astrophysics*, *377*, 297–311. https://doi.org/10.1051/0004-6361:20011056